Eur. Phys. J. C (2022) 82:483
https://doi.org/10.1140/epjc/s10052-022-10414-w

THE EUROPEAN PHYSICAL JOURNAL C

Regular Article - Theoretical Physics

$(g-2)_\mu$ and SUSY dark matter: direct detection and collider search complementarity

Manimala Chakraborti[1,a], **Sven Heinemeyer**[2,b], **Ipsita Saha**[3,c], **Christian Schappacher**[4,d]

[1] Astrocent, Nicolaus Copernicus Astronomical Center of the Polish Academy of Sciences, ul. Rektorska 4, 00-614 Warsaw, Poland
[2] Instituto de Física Teórica (UAM/CSIC), Universidad Autónoma de Madrid, Cantoblanco, 28049 Madrid, Spain
[3] Kavli IPMU (WPI), UTIAS, University of Tokyo, Kashiwa, Chiba 277-8583, Japan
[4] Institut für Theoretische Physik, Karlsruhe Institute of Technology, 76128 Karlsruhe, Germany

Received: 15 December 2021 / Accepted: 10 May 2022 / Published online: 25 May 2022

Abstract The electroweak (EW) sector of the Minimal Supersymmetric Standard Model (MSSM) can account for a variety of experimental data. The EW particles with masses of a few hundred GeV evade the LHC searches owing to their small production cross sections. Such a light EW sector can in particular explain the reinforced $4.2\,\sigma$ discrepancy between the experimental result for the anomalous magnetic moment of the muon, $(g-2)_\mu$, and its Standard Model (SM) prediction. The lightest supersymmetric particle (LSP), assumed to be the lightest neutralino, $\tilde{\chi}_1^0$, as a Dark Matter (DM) candidate is furthermore in agreement with the observed limits on the DM content of the universe. Here the Next-to LSP (NLSP) serves as a coannihilation partner and is naturally close in mass to the LSP. Such scenarios are also to a large extent in agreement with negative results from Direct Detection (DD) experiments. The DM relic density can fully be explained by a nearly pure bino or a mixed bino/wino LSP. Relatively light wino and higgsino DM, on the other hand, remains easily below the DM relic density upper bound. Using the improved limits on $(g-2)_\mu$, we explore the mass ranges of the LSP and the NLSP in their correlation with the DM relic density for bino, bino/wino, wino and higgsino DM. In particular, we analyze the sensitivity of future DM DD experiments to these DM scenarios. We find that higgsino, wino and one type of bino scenario can be covered by future DD experiments. Mixed bino/wino and another type of bino DM can reach DD cross sections below the neutrino floor. In these cases we analyze the complementarity with the (HL-)LHC and future e^+e^- linear colliders. We find that while the prospects for the HL-LHC are interesting, but not conclusive, an e^+e^- collider with $\sqrt{s} \lesssim 1$ TeV can cover effectively all points of the MSSM that may be missed by DD experiments.

1 Introduction

Searches for Dark Matter (DM) is one of the main objectives in today's particle and astroparticle physics. Searches at the LHC (or other collider experiments) are complementary to the searches in "direct detection" (DD) experiments. Among the Beyond the Standard Model (BSM) theories that predict a viable DM particle the Minimal Supersymmetric Standard Model (MSSM) [1–4] is one of the leading candidates. Supersymmetry (SUSY) predicts two scalar partners for all Standard Model (SM) fermions as well as fermionic partners to all SM bosons. Furthermore, contrary to the SM case, the MSSM requires two Higgs doublets. This results in five physical Higgs bosons instead of the single Higgs boson in the SM: the light and heavy $\mathcal{CP}$-even Higgs bosons, h and H, the $\mathcal{CP}$-odd Higgs boson, A, and the charged Higgs bosons, $H^\pm$. The neutral SUSY partners of the (neutral) Higgs and electroweak (EW) gauge bosons gives rise to the four neutralinos, $\tilde{\chi}_{1,2,3,4}^0$. The corresponding charged SUSY partners are the charginos, $\tilde{\chi}_{1,2}^\pm$. The SUSY partners of the SM leptons and quarks are the scalar leptons and quarks (sleptons, squarks), respectively. The lightest SUSY particle (LSP) is naturally the lightest neutralino, $\tilde{\chi}_1^0$. It can make up the full DM content of the universe [5,6], or, depending on its nature only a fraction of it. In the latter case, an additional DM component could be, e.g., a SUSY axion [7], which would then bring the total DM density into agreement with the experimental measurement.

In Refs. [8–10] we performed a comprehensive analysis of the EW sector of the MSSM, taking into account all relevant theoretical and experimental constraints. The experimental

[a] e-mail: mani.chakraborti@gmail.com (corresponding author)
[b] e-mail: Sven.Heinemeyer@cern.ch
[c] e-mail: ipsita.saha@ipmu.jp
[d] e-mail: schappacher@kabelbw.de

results comprised the direct searches at the LHC [11,12], the DM relic abundance [13] (either as an upper limit [9] or as a direct measurement [8,10]), the DM direct detection (DD) experiments [14–16] and in particular the deviation of the anomalous magnetic moment of the muon (either the previous result [8,9], or the new, stronger limits [10]). Five different scenarios were analyzed, classified by the mechanism that brings the LSP relic density into agreement with the measured values. The scenarios differ by the Next-to-LSP (NLSP), or equivalently by the mass hierarchies between the mass scales determining the neutralino, chargino and slepton masses. These mass scales are the gaugino soft-SUSY breaking parameters M_1 and M_2, the Higgs mixing parameter μ and the slepton soft SUSY-breaking parameters $m_{\tilde{l}_L}$ and $m_{\tilde{l}_R}$, see Sect. 2 for a detailed description. The five scenarios can be summarized as follows [8–10]:

(i) higgsino DM ($\mu < M_1, M_2, m_{\tilde{l}_L}, m_{\tilde{l}_R}$), DM relic density is only an upper bound (the full relic density implies $m_{\tilde{\chi}_1^0} \sim 1$ TeV and $(g-2)_\mu$ cannot be fulfilled), $m_{\text{(N)LSP}} \lesssim 500$ GeV with $m_{\text{NLSP}} - m_{\text{LSP}} \sim 5$ GeV;
(ii) wino DM ($M_2 < M_1, \mu, m_{\tilde{l}_L}, m_{\tilde{l}_R}$), DM relic density is only an upper bound, (the full relic density implies $m_{\tilde{\chi}_1^0} \sim 3$ TeV and $(g-2)_\mu$ cannot be fulfilled), $m_{\text{(N)LSP}} \lesssim 600$ GeV with $m_{\text{NLSP}} - m_{\text{LSP}} \sim 0.3$ GeV;
(iii) bino/wino DM with $\tilde{\chi}_1^\pm$-coannihilation ($M_1 \lesssim M_2$), DM relic density can be fulfilled, $m_{\text{(N)LSP}} \lesssim 650\,(700)$ GeV;
(iv) bino DM with $\tilde{l}^\pm$-coannihilation case-L ($M_1 \lesssim m_{\tilde{l}_L}$), DM relic density can be fulfilled, $m_{\text{(N)LSP}} \lesssim 650\,(700)$ GeV;
(v) bino DM with $\tilde{l}^\pm$-coannihilation case-R ($M_1 \lesssim m_{\tilde{l}_R}$), DM relic density can be fulfilled, $m_{\text{(N)LSP}} \lesssim 650\,(700)$ GeV.

Recently the "MUON G-2" collaboration published the results of their Run 1 data [17], which is within $0.8\,\sigma$ in agreement with the older BNL result on $(g-2)_\mu$ [18]. The combined measurement yields a deviation from the SM prediction of $\Delta a_\mu = (25.1 \pm 5.9) \times 10^{-10}$, corresponding to $4.2\,\sigma$. Imposing this limit on the MSSM parameter space allows to set *upper* limits on the EW sector. Here it is interesting to note that the old lower $2\,\sigma$ limit on Δa_μ, $\Delta a_\mu^{-2\,\sigma,\text{old}} = 12.9 \times 10^{-10}$, coincidentally agrees quite well with the new lower limit, $\Delta a_\mu^{-2\,\sigma} = 13.3 \times 10^{-10}$. Consequently, the new combined a_μ result confirmed the *upper* mass limits obtained with the old a_μ result at a higher confidence level. While in Refs. [8,9] the old deviation (i.e. without the new "MUON G-2" result) was used for scenarios (i)-(v), scenarios (iii)-(v) have been updated with the new result in Ref. [10]. Other evaluations within the framework of SUSY using the new combined deviation Δa_μ can be found in Refs. [19–61].

In this letter we address the implications of the new result for Δa_μ for the DM predictions in the five scenarios. The main idea is to analyze for the five scenarios the complementarity of DD experiments and future collider experiments, concretely the HL-LHC and a possible future linear e^+e^- collider, the International Linear Collider (ILC), operated at a center-of-mass energy of up to $\sqrt{s} \lesssim 1$ TeV, the ILC1000. In the first step we will analyze the predictions for the DM relic density as a function of the (N)LSP masses. Here, in scenarios (iii)-(v) we will show the results both for DM fulfilling the relic density, as well as taking the DM density only as an upper bound. In scenarios (i) and (ii), we analyze the case where a fraction of DM relic density is contributed by $\tilde{\chi}_1^0$ while being in agreement with the Δa_μ requirement. In the second step we evaluate the prospects for future DD experiments in these five scenarios. We show that higgsino, wino and bino case-R DM can be covered by the future DD experiments. Mixed bino/wino DM and bino case-L DM, on the other hand, can reach DD cross sections below the neutrino floor for a significant amount of model parameter space, if the DM relic density remains substantially below the Planck measurement. In this case direct searches at the HL-LHC and particularly at the ILC1000 will be necessary to fully cover these scenarios. While Refs. [19–61] study the Δa_μ implications in SUSY models, to our knowledge a DM analysis, particularly in view of the future detection prospect, as performed here, has not been done.

2 The electroweak sector of the MSSM

In our notation for the MSSM we follow exactly Ref. [8]. Here we restrict ourselves to a very short introduction of the relevant parameters and symbols of the EW sector of the MSSM, consisting of charginos, neutralinos and scalar leptons. For the scalar quark sector, we assume it to be heavy and not to play a relevant role in our analysis. Throughout this paper we also assume absence of $\mathcal{CP}$-violation, i.e. that all parameters are real.

The masses and mixings of the neutralinos are set (on top of SM parameters) by the $U(1)_Y$ and $SU(2)_L$ gaugino masses, M_1 and M_2, the Higgs mixing parameter μ, as well as the ratio of the two vacuum expectation values (vevs) of the two Higgs doublets, $\tan\beta := v_2/v_1$. After the diagonalization of the mass matrix the four eigenvalues give the four neutralino masses $m_{\tilde{\chi}_1^0} < m_{\tilde{\chi}_2^0} < m_{\tilde{\chi}_3^0} < m_{\tilde{\chi}_4^0}$. Similarly, the masses and mixings of the charginos are set (on top of SM parameters) by M_2, μ and $\tan\beta$. The diagonalization of the mass matrix yields the two chargino-mass eigenvalues $m_{\tilde{\chi}_1^\pm} < m_{\tilde{\chi}_2^\pm}$.

For the sleptons, as in Ref. [8], we have chosen common soft SUSY-breaking parameters for all three generations. The charged slepton mass matrix are given (on top of SM parameters) by the diagonal soft SUSY-breaking parameters $m^2_{\tilde{l}_L}$ and $m^2_{\tilde{l}_R}$ and the trilinear Higgs-slepton coupling A_l ($l = e, \mu, \tau$), where the latter are set to zero. Mixing between the "left-handed" and "right-handed" sleptons is only relevant for staus, where the off-diagonal entry in the mass matrix is dominated by $-m_\tau \mu \tan\beta$. Consequently, for the first two generations, the mass eigenvalues can be approximated as $m_{\tilde{l}_1} \simeq m_{\tilde{l}_L}, m_{\tilde{l}_2} \simeq m_{\tilde{l}_R}$ (assuming small D-terms). In general we follow the convention that $\tilde{l}_1$ ($\tilde{l}_2$) has the large "left-handed" ("right-handed") component, i.e. they are not mass ordered. Besides the symbols are equal for all three generations, $m_{\tilde{l}_1}$ and $m_{\tilde{l}_2}$, we also use symbols for the scalar electron, muon and tau masses, $m_{\tilde{e}_{1,2}}$, $m_{\tilde{\mu}_{1,2}}$ and $m_{\tilde{\tau}_{1,2}}$. The sneutrino and slepton masses are connected by the usual SU(2) relation.

Overall, the EW sector at the tree level can be described with the help of six parameters: M_1, M_2, μ, $\tan\beta$, $m_{\tilde{l}_L}$ and $m_{\tilde{l}_R}$. Throughout our analysis we assume $\mu, M_1, M_2 > 0$. In Ref. [8] it was shown that choosing these parameters positive covers the relevant parameter space once the $(g-2)_\mu$ results are taken into account (see, however, the discussion in Ref. [31]).

Following the experimental limits from the LHC [11,12] for strongly interacting particles, we assume that the colored sector of the MSSM is substantially heavier than the EW sector, and thus does not play a role in our analysis. For the Higgs-boson sector we assume that the radiative corrections to the light $\mathcal{CP}$-even Higgs boson, which largely originate from the top/stop sector, yield a value in agreement with the experimental data, $M_h \sim 125$ GeV. This yields stop masses naturally in the TeV range [62,63], in agreement with the LHC bounds. Concerning the heavy Higgs-boson mass scale, as given by M_A, the $\mathcal{CP}$-odd Higgs-boson mass, we have shown in Refs. [8–10] that A-pole annihilation is largely excluded. Consequently, we simply assume M_A to be sufficiently large to not play a role in our analysis.

3 Relevant constraints

The SM prediction of a_μ is given by [64] (based on Refs. [65–84]),[1]

$$a_\mu^{\rm SM} = (11659181.0 \pm 4.3) \times 10^{-10}\,. \tag{1}$$

The combined experimental new world average, based on Refs. [17,18], was announced as

$$a_\mu^{\rm exp} = (11659206.1 \pm 4.1) \times 10^{-10}. \tag{2}$$

Compared with the SM prediction in Eq. (1), one arrives at a new deviation of

$$\Delta a_\mu = (25.1 \pm 5.9) \times 10^{-10}, \tag{3}$$

corresponding to a 4, 2, σ discrepancy. We use this limit as a cut at the $\pm 2\,\sigma$ level.

Recently a new lattice calculation for the leading order hadronic vacuum polarization (LO HVP) contribution to $a_\mu^{\rm SM}$ [85] has been reported, which, however, was not used in the new theory world average, Eq. (1) [64]. Consequently, we also do not take this result into account, see also the discussions in Refs. [8,85–89]. On the other hand, it is obvious that our conclusions would change substantially if the result presented in [85] turned out to be correct.

In the MSSM the main contribution to $(g-2)_\mu$ comes from one-loop diagrams involving $\tilde{\chi}_1^\pm - \tilde{\nu}$ and $\tilde{\chi}_1^0 - \tilde{\mu}$ loops. In our analysis the MSSM contribution to $(g-2)_\mu$ at two-loop order is calculated using `GM2Calc` [90], implementing two-loop corrections from [91–93] (see also [94,95]).

All other constraints are taken into account exactly as in Refs. [8–10]. These are

- Vacuum stability constraints:
  All points are checked to possess a stable and correct EW vacuum, e.g. avoiding charge and color breaking minima. This check is performed with the public code `Evade` [96,97].
- Constraints from the LHC:
  All relevant SUSY searches for EW particles are taken into account, mostly via `CheckMATE` [98–100] (see Ref. [8] for details on many analyses newly implemented by our group). The LHC constraints that are most important for our scenarios come from i) the production of $\tilde{\chi}_1^\pm - \tilde{\chi}_2^0$ pairs leading to three leptons and $\not{E}_T$ in the final state [101] ii) slepton-pair production leading to two same flavour opposite sign leptons and $\not{E}_T$ in the final state [102]. Since all of our scenarios feature a low mass gap between the LSP and the NLSP, the compressed spectra searches with the signature of two soft leptons and $\not{E}_T$ accompanied by an initial state radiation (ISR) jet [103] also prove to be relevant in this case. For the wino case, the disappearing track searches [104,105] are useful especially in the region of a low mass gap, $\Delta m \sim$ a few hundred MeV.
- Dark matter relic density constraints:
  For the experimental data we use the latest result from Planck [13], either as a direct measurement,

$$\Omega_{\rm CDM} h^2 \;=\; 0.120, \pm 0.001, \tag{4}$$

[1] In Ref. [8] a slightly different value was used, with a negligible effect on the results.

or as an upper bound,

$$\Omega_{\rm CDM}h^2 \;\leq\; 0.120. \tag{5}$$

The relic density in the MSSM is evaluated with MicrOMEGAs [106–109]. In the latter case one needs an additional DM component which would then bring the total DM density into agreement with the Planck measurement in Eq. (4). This could be, e.g., a SUSY axion [7]. In the case of wino DM, because of the extremely small mass splitting, the effect of "Sommerfeld enhancement" [110] can be very important. However, in Ref. [9] we argued why this does not have any relevant effect on our analysis, and thus we do not take it into account.

- Direct detection constraints of Dark matter:
  We employ the constraint on the spin-independent (SI) DM scattering cross-section $\sigma_p^{\rm SI}$ from XENON-1T [14] experiment (which are always substantially more relevant than the spin-dependent limits). The theoretical predictions are evaluated using the public code MicrOMEGAs [106–109]. A combination with other DD experiments would put only very slightly stronger limits. However, we will discuss the impact of possible future limits and the neutrino floor below.
  Here it should be noted that for parameter points with $\Omega_{\tilde\chi}h^2 \;\leq\; 0.118$ (i.e. $2\,\sigma$ lower than the limit from Planck [13], see Eq. (5)) we rescale the cross-section with a factor of $(\Omega_{\tilde\chi}h^2/0.118)$ to take into account the fact that $\tilde\chi_1^0$ provides only a fraction of the total DM relic density of the universe.

Another potential set of constraints is given by the indirect detection of DM. However, we do not impose these constraints on our parameter space because of the well-known large uncertainties associated with astrophysical factors like DM density profile as well as theoretical corrections, see Refs. [111–114].

4 Parameter scan and analysis flow

4.1 Parameter scan

We scan the relevant MSSM parameter space to fully cover the allowed regions of the relevant neutralino, chargino and slepton masses. We follow the approach taken in Refs. [8–10] and investigate the five scenarios listed in Sect. 1. They are given by the possible mass orderings of M_1, M_2, μ and $m_{\tilde l_L}$, $m_{\tilde l_R}$. These masses determine the nature of the LSP and the NLSP, and thus also the mechanism that reduces the relic DM density in the early universe to or below the current value, see Eqs. (4), (5), i.e. coannihilation with the NLSP. We do not take into account the possibility of pole annihilation, e.g. with the A, the h or the Z boson. As argued in Refs. [8–10] these are rather remote possibilities in our set-up. [2] The five cases are covered as follows.

(A) Higgsino DM
This scenario is characterized by a small value of μ (as favored, e.g., by naturalness arguments [115–120]).[3] Such a scenario is also naturally realized in Anomaly Mediation SUSY breaking (AMSB, see e.g. Ref. [122] and references therein). We scan the following parameters:

$$\begin{aligned} &100\ \text{GeV} \leq \mu \leq 1200\ \text{GeV}, \quad 1.1\mu \leq M_1, M_2 \leq 10\mu, \\ &5 \leq \tan\beta \leq 60, \quad 100\,\text{GeV} \leq m_{\tilde l_L}, m_{\tilde l_R} \leq 2000\ \text{GeV}. \end{aligned} \tag{6}$$

(B) Wino DM
This scenario is characterized by a small value of M_2. Also this type of scenario is naturally realized in the AMSB (see e.g. Ref. [122] and references therein). We scan the following parameters:

$$\begin{aligned} &100\ \text{GeV} \leq M_2 \leq 1500\,\text{GeV}, \quad 1.1M_2 \leq M_1, \mu \leq 10M_2, \\ &5 \leq \tan\beta \leq 60, \quad 100\,\text{GeV} \leq m_{\tilde l_L}, m_{\tilde l_R} \leq 2000\ \text{GeV}. \end{aligned} \tag{7}$$

Here it should be noted that the choice of $M_2 \ll M_1, \mu$ at tree-level leads to an almost degenerate spectrum with $m_{\tilde\chi_1^\pm} - m_{\tilde\chi_1^0} = \mathcal{O}(1\,\text{eV})$. Going to the on-shell (OS) masses, yielding a mass shift in $m_{\tilde\chi_1^0}$ and two other neutralino masses, the mass splitting between $m_{\tilde\chi_1^\pm}$ and $m_{\tilde\chi_1^0}$ is elevated which subsequently allows the decay $\tilde\chi_1^\pm \to \tilde\chi_1^0\pi^\pm$. We refer to Ref. [9] for a detailed description of our procedure. [4]

(C) Mixed bino/wino DM
Here we choose M_1 to be the smallest mass parameter and require $\tilde\chi_1^\pm$-coannihilation, given by a relatively small M_2. The scan parameters are chosen as,

$$\begin{aligned} &100\ \text{GeV} \leq M_1 \leq 1000\ \text{GeV}, \quad M_1 \leq M_2 \leq 1.1M_1, \\ &1.1M_1 \leq \mu \leq 10M_1, \quad 5 \leq \tan\beta \leq 60, \\ &100\ \text{GeV} \leq m_{\tilde l_L} \leq 1500\ \text{GeV}, \quad m_{\tilde l_R} = m_{\tilde l_L}. \end{aligned} \tag{8}$$

(D) Bino DM
Also in this scenario we choose M_1 to be the smallest

[2] Concretely, we have set $M_A = 1.5$ TeV, which ensures that the heavy Higgs-boson sector does not play a role in our analysis.

[3] See Ref. [121] for a recent analysis in the higgsino DM scenario, requiring the LSP to yield the full DM relic density.

[4] The mass shift for our wino DM points has been calculated following Refs. [123,124].

mass parameter, but now require that a slepton is close in mass. In this scenario "accidentally" the wino component of the $\tilde{\chi}_1^0$ can be non-negligible. However, this is not a distinctive feature of this scenario. We distinguish two cases: either the SU(2) doublet sleptons, or the singlet sleptons are close in mass to the LSP.

(D1) case-L: SU(2) doublet

$$\begin{aligned} &100\ \text{GeV} \leq M_1 \leq 1000\ \text{GeV}, \quad M_1 \leq M_2 \leq 10M_1, \\ &1.1M_1 \leq \mu \leq 10M_1, \quad 5 \leq \tan\beta \leq 60, \\ &M_1 \leq m_{\tilde{l}_L} \leq 1.2M_1, \quad M_1 \leq m_{\tilde{l}_R} \leq 10M_1. \end{aligned} \tag{9}$$

(D2) case-R: SU(2) singlet

$$\begin{aligned} &100\ \text{GeV} \leq M_1 \leq 1000\ \text{GeV}, \quad M_1 \leq M_2 \leq 10M_1, \\ &1.1M_1 \leq \mu \leq 10M_1, \quad 5 \leq \tan\beta \leq 60, \\ &M_1 \leq m_{\tilde{l}_L} \leq 10M_1, \quad M_1 \leq m_{\tilde{l}_R} \leq 1.2M_1. \end{aligned} \tag{10}$$

In all scans we choose flat priors of the parameter space and generate $\mathcal{O}(10^7)$ points.

As discussed above, the mass parameters of the colored sector have been set to high values, such that the resulting SUSY particle masses are outside the reach of the LHC, and the light $\mathcal{CP}$-even Higgs-boson is in agreement with the LHC measurements of the $\sim$ 125 GeV Higgs boson, where the concrete values are not relevant for our analysis. Also M_A has been set to be above the TeV scale.

4.2 Analysis flow

The data samples are generated by scanning randomly over the input parameter range given above, where a flat prior has been taken for all parameters. We use `SuSpect` [125] as spectrum and SLHA file generator. In the next step the parameter points are required to satisfy the $\tilde{\chi}_1^\pm$ mass limit from LEP [126]. The SLHA output files as generated by `SuSpect` are then passed as input files to `GM2Calc` and `MicrOMEGAs` for the calculation of $(g-2)_\mu$ and the DM observables, respectively. The parameter points that satisfy the new $(g-2)_\mu$ constraint, Eq. (3), the DM relic density, Eq. (4) or (5) (depending on the scenario), the direct detection constraints (possibly with a rescaled cross section) and the vacuum stability constraints, checked with `Evade`, are then taken to the final check against the LHC constraints as implemented in `CheckMATE`. The relevant branching ratios of the SUSY particles required by `CheckMATE` are computed using `SDECAY` [127].

5 Results

In this section we present our results for the DM implications in the five scenarios. For each scenario we show the preferred ranges for the LSP and NLSP masses, the DM relic density and the prospects for future DD experiments.

5.1 Higgsino DM

We start our discussion with the case of higgsino DM, as defined in Sect. 4.1. The plots show only points that are in agreement with all theoretical and experimental constraints.

In Fig. 1 we show the results of our parameter scan. The upper plot shows the $m_{\tilde{\chi}_1^0}$–Δm plane, with $\Delta m := m_{\tilde{\chi}_1^\pm} - m_{\tilde{\chi}_1^0}$, and $m_{\tilde{\chi}_2^0} \approx m_{\tilde{\chi}_1^\pm}$. The allowed LSP masses range from $\sim$ 150 GeV to about $\sim$ 500 GeV, where Δm is found in the range between $\sim$ 1.5 GeV and $\sim$ 7 GeV. Larger DM masses are reached for smaller mass gaps. The color code indicates

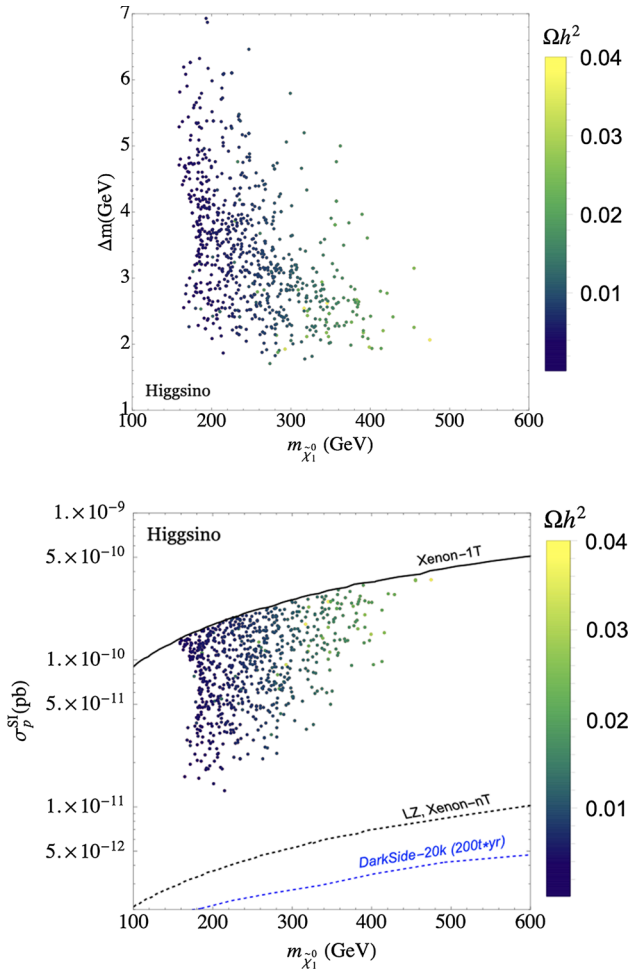

Fig. 1 The results of our parameter scan in the higgsino DM scenario. Upper plot: $m_{\tilde{\chi}_1^0}$–Δm plane ($\Delta m = m_{\tilde{\chi}_1^\pm} - m_{\tilde{\chi}_1^0}$). Lower plot: $m_{\tilde{\chi}_1^0}$–σ_p^{SI} plane. The color code indicates the DM relic density

the relic density. Low LSP masses correspond to the lowest density, below $\Omega_{\tilde{\chi}_1^0}h^2 \lesssim 0.01$, going up to ~ 0.04 for the largest values of $m_{\tilde{\chi}_1^0}$. The full relic density would be reached for $m_{\tilde{\chi}_1^0} \sim 1$ TeV. This, however, would be in disagreement with the $(g-2)_\mu$ prediction, and consequently, only lower densities are found.

We now turn to the prediction for the direct detection of DM in the higgsino scenario. Here it is important to note that the dominant contribution to DM scattering comes from the exchange of a light $\mathcal{CP}$-even Higgs boson in the t-channel. The corresponding $h\tilde{\chi}_1^0\tilde{\chi}_1^0$ coupling is given at tree level by [128]

$$c_{h\tilde{\chi}_1^0\tilde{\chi}_1^0} \simeq -\frac{1}{2}(1+\sin 2\beta)\left(\tan^2\theta_{\rm w}\frac{M_W}{M_1-\mu}+\frac{M_W}{M_2-\mu}\right), \tag{11}$$

where $\mu > 0$ has been assumed (as given in our scan). One can see that the coupling becomes large for $\mu \sim M_2$ or $\mu \sim M_1$. Consequently, the XENON-1T DD bound pushes the allowed parameter space into the almost pure higgsino-LSP region, with negligible bino and wino component, i.e. to larger values for M_2/μ and M_1/μ. This also suppresses the $Z\tilde{\chi}_1^0\tilde{\chi}_1^0$ coupling, which is responsible for the spin-dependent (SD) interaction between $\tilde{\chi}_1^0$ and the nucleons [128]. Therefore, our parameter space is not restricted by the bounds on SD DD cross-section. We have checked explicitly that all of our points lie well below the latest constraints on the $\sigma_{p,n}^{\rm SD}$ from the experiments like PICO60 [129] and XENON1T [130]. Consequently, in our analysis we focus on the prospects for SI DD bounds on our parameter space.

In the lower plot of Fig. 1 we show the prediction for the direct detection prospects in the higgsino DM scenario. The allowed points are displayed in the $m_{\tilde{\chi}_1^0}$–$\sigma_p^{\rm SI}$ plane, where again the color code indicates the DM relic density. Here it should be remembered that we rescale the cross-section with a factor of $(\Omega_{\tilde{\chi}}h^2/0.118)$ to take into account the fact that $\tilde{\chi}_1^0$ provides only a fraction of the total DM relic density of the universe. The points are by construction bounded from above by the XENON-1T limit [14]. We also show the projection for the exclusion reach of XENON-nT [131] and of the LZ experiment [132] as black dashed line (which effectively agree with each other). Furthermore, we show the projection of the DarkSide [133] experiment, which can go down to even lower cross sections, as blue dashed line. One can see that the full parameter space will be covered already by XENON-nT and/or LZ. Also DarkSide with its lower reach will cover the complete higgsino DM scenario.

5.2 Wino DM

The next case we present here is the wino DM case, as discussed in Sect. 4.1. As before, the plots show only points that are in agreement with all theoretical and experimental constraints.

In Fig. 2 we show the results of our parameter scan. The upper plot shows the $m_{\tilde{\chi}_1^0}$–Δm plane, with $\Delta m := m_{\tilde{\chi}_1^\pm} - m_{\tilde{\chi}_1^0}$. The allowed LSP masses range from $\sim$ 100 GeV, where we started our scan, to about $\sim$ 600 GeV, where Δm is found in the range between $\sim$ 0.2 GeV and $\sim$ 2 GeV. Here it should be remembered that the choice of $M_2 \ll M_1, \mu$ leads to an approximately degenerate spectrum at tree-level with $m_{\tilde{\chi}_1^\pm} - m_{\tilde{\chi}_1^0} = \mathcal{O}(1\,\text{eV})$. Only by going to OS masses, yielding a mass shift in $m_{\tilde{\chi}_1^0}$ and two other neutralino masses and hence with the raised splitting between $m_{\tilde{\chi}_1^\pm}$ and $m_{\tilde{\chi}_1^0}$, the decay $\tilde{\chi}_1^\pm \to \tilde{\chi}_1^0\pi^\pm$ is allowed. The disappearing track searches at the LHC [105] then cut away the smallest Δm region (see Ref. [9] for details), resulting in the lower limit displayed in Fig. 2. Larger DM masses are reached for smaller mass gaps. The color code indicates the relic density. Low LSP masses correspond to the lowest density, below $\Omega_{\tilde{\chi}_1^0}h^2 \lesssim 0.0025$ (i.e. even smaller by a factor of four compared to the higgsino case), going up to $\sim$ 0.015 for the largest values of $m_{\tilde{\chi}_1^0}$. The full relic density would be reached for $m_{\tilde{\chi}_1^0} \sim 3$ TeV. However, as in the higgsino case, this would be in disagreement with the $(g-2)_\mu$ prediction, and consequently, only substantially lower densities are found.

The overall allowed parameter space is furthermore bounded from "above" by the DD limits, which cut away larger mass differences, which can be understood as follows. For a wino-like $\tilde{\chi}_1^0$, the $h\tilde{\chi}_1^0\tilde{\chi}_1^0$ coupling is given by [128]

$$c_{h\tilde{\chi}_1^0\tilde{\chi}_1^0} \simeq \frac{M_W}{M_2^2-\mu^2}(M_2+\mu\sin 2\beta). \tag{12}$$

In the limit of $||\mu| - M_2| \gg M_Z$ and assuming also that the h-exchange dominates over the H contribution in the (spin independent) DD bounds (i.e. the $\mathcal{CP}$-odd Higgs also does not contribute), the $h\tilde{\chi}_1^0\tilde{\chi}_1^0$ coupling becomes large at $\mu \sim M_2$. The tree level mass splitting between the two wino-like states $\tilde{\chi}_1^\pm$ and $\tilde{\chi}_1^0$ (generated mainly by the mixing of the lighter chargino with the charged higgsino) is given by [134]

$$\Delta m (= m_{\tilde{\chi}_1^\pm} - m_{\tilde{\chi}_1^0}) \simeq \frac{M_W^4(\sin 2\beta)^2\tan^2\theta_{\rm w}}{(M_1-M_2)\mu^2}, \tag{13}$$

assuming $|M_1 - M_2| \gg M_Z$. Therefore, the mass splitting increases for smaller μ values with a simultaneous increase in DD cross-section.

In the lower plot of Fig. 2 we show the prediction for the direct detection prospects in the wino DM scenario. The allowed points are displayed in the $m_{\tilde{\chi}_1^0}$–$\sigma_p^{\rm SI}$ plane, where again the color code indicates the DM relic density. As in the higgsino DM case we re-scale the cross-section with a factor of $(\Omega_{\tilde{\chi}}h^2/0.118)$ to take into account the fact that $\tilde{\chi}_1^0$ provides only a fraction of the total DM relic density of the universe. By construction the points are bounded from above by the

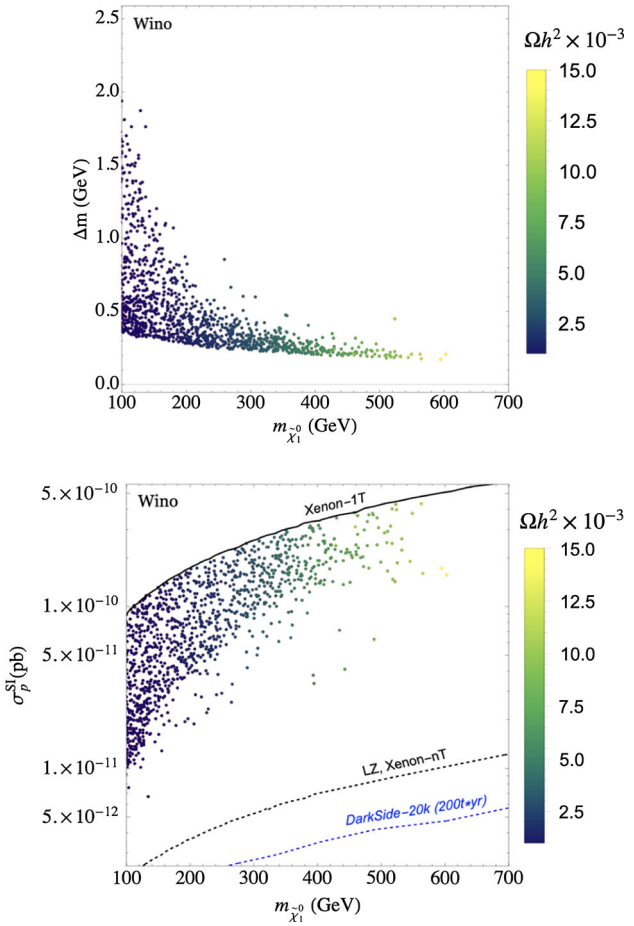

Fig. 2 The results of our parameter scan in the wino DM scenario. Upper plot: $m_{\tilde{\chi}_1^0}$–Δm plane ($\Delta m = m_{\tilde{\chi}_1^\pm} - m_{\tilde{\chi}_1^0}$). Lower plot: $m_{\tilde{\chi}_1^0}$–$\sigma_p^{\rm SI}$ plane. The color code indicates the DM relic density

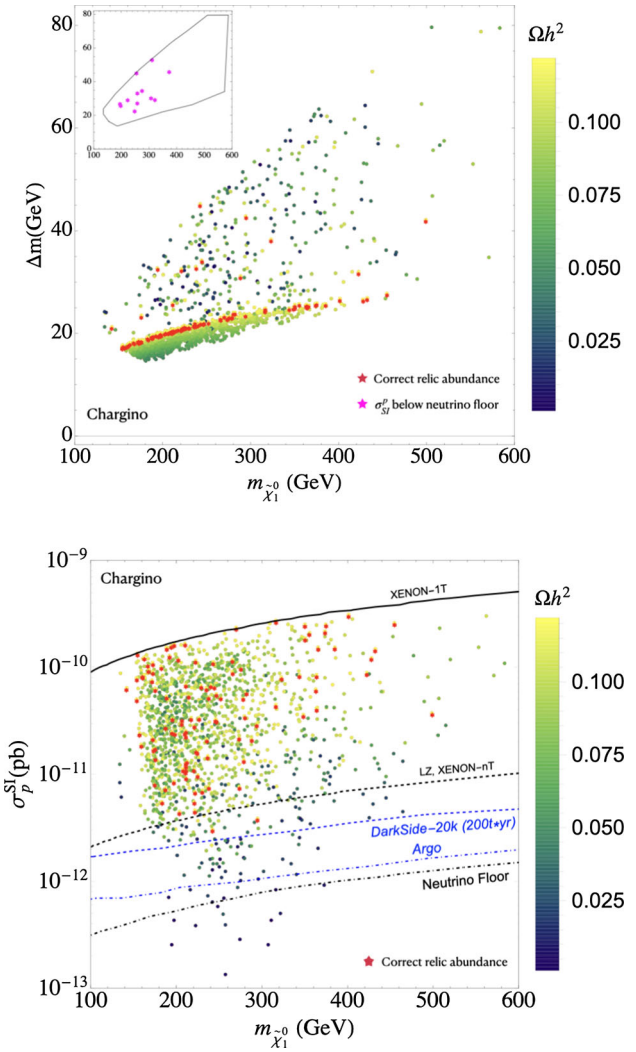

Fig. 3 The results of our parameter scan in the bino/wino DM scenario with $\tilde{\chi}_1^\pm$-coannihilation. Upper plot: $m_{\tilde{\chi}_1^0}$–Δm plane ($\Delta m = m_{\tilde{\chi}_1^\pm} - m_{\tilde{\chi}_1^0}$). Lower plot: $m_{\tilde{\chi}_1^0}$–$\sigma_p^{\rm SI}$ plane. The color code indicates the DM relic density. Red points are in full agreement with the Planck measurement. The magenta points shown in the inlay in the upper plot indicate the points below the neutrino floor, where the solid line indicates the overall allowed parameter space

XENON-1T limit [14], where the smallest μ/M_2 values are found. As discussed above, the lower limit is given by the disappearing track searches at the LHC [105], i.e. small mass splittings. Also in this plot we show as black dashed line the projected limit of XENON-nT/LZ and as blue dashed line the one of DarkSide. One can see that the XENON-nT and/or LZ result will either firmly exclude or detect a wino DM candidate, possibly in conjunction with improved disappearing track searches at the LHC. The same holds for the DarkSide experiment.

5.3 Bino/wino DM with $\tilde{\chi}_1^\pm$-coannihilation

In this section we analyze the case of bino/wino DM, as defined in Sect. 4.1. In this scenario $\tilde{\chi}_1^\pm$-coannihilation is responsible for finding the DM relic density either in full agreement with the Planck measurements, see Eq. (4), or is found to be smaller, see Eq. (5).

In the upper plot of Fig. 3 we show our results in the $m_{\tilde{\chi}_1^0}$–Δm plane (with $\Delta m = m_{\tilde{\chi}_1^\pm} - m_{\tilde{\chi}_1^0}$). The color coding indicates the DM relic density, where the red points correspond to full agreement with the Planck measurement, see Eq. (4). The magenta points shown in the inlay are found below the neutrino floor, see the discussion below. The solid line surrounding the points indicates the overall allowed parameter space in this plane. By definition of $\tilde{\chi}_1^\pm$-coannihilation, the points are found for relatively low values of Δm, between $\sim$ 10 GeV and $\sim$ 60 GeV. Two "populations" can be observed. One large group of parameter points are found at $\Delta m \sim 20$ GeV. In these points only the chargino contributes relevantly to the correct relic abundance. For the sparsely distributed region in the higher Δm, mostly sleptons contribute to the coannihilation. Concerning the "pure" $\tilde{\chi}_1^\pm$-coannihilation points, due

to the small mass splitting, it will be more complicated to detect these points at the (HL-)LHC, see also the discussion in Sect. 6.1.

The prediction for the DD experiments is demonstrated in the lower plot of Fig. 3. We show the $m_{\tilde{\chi}_1^0}$–$\sigma_p^{\rm SI}$ plane, again with the color coding indicating the DM relic density. As in the previous cases, for the points with a lower relic density we rescale the cross-section with a factor of $(\Omega_{\tilde{\chi}} h^2/0.118)$ to take into account the fact that $\tilde{\chi}_1^0$ provides only a fraction of the total DM relic density of the universe. By construction, the upper limit of the points is provided by the XENON-1T limit. In addition to the XENON-nT, LZ and DarkSide limits we also show the anticipated reach of the Argo experiment [135], as well as the neutrino floor [136]. It is evident that for the lowest DM relic density, the DD cross-section is considerably scaled down. The red points, i.e. the ones with correct relic abundance, spread out even slightly below the future XENON-nT/LZ limit, but all lie above the anticipated reach of DarkSide and Argo. Cross sections lower than the DarkSide reach are only found for low values of $\Omega_{\tilde{\chi}} h^2$. Those points can reach even values below the neutrino floor. As can be seen in the inlay in the upper plot of Fig. 3, these points (indicated by magenta stars) do not exceed $m_{\tilde{\chi}_1^0} \sim 400$ GeV. On the other hand, no clear pattern w.r.t. Δm can be observed for these points. In Sect. 6 we will discuss the complementarity of the direct detection experiments with the anticipated reach at the (HL-)LHC and possible future e^+e^- collider experiments. From the upper limit on the masses of the points below the neutrino floor, it becomes apparent already that one could cover them at an e^+e^- collider with $\sqrt{s} \lesssim 1$ TeV via $e^+e^- \to \tilde{\chi}_1^0 \tilde{\chi}_1^0 \gamma$. This demonstrates the complementarity of DD experiments and future (linear) e^+e^- colliders.

5.4 Bino DM with $\tilde{l}^{\pm}$-coannihilation case-L

We now turn to the case of bino DM with $\tilde{l}^{\pm}$-coannihilation. As discussed in Sect. 4.1 we distinguish two cases, depending which of the two slepton soft SUSY-breaking parameters is set to be close to $m_{\tilde{\chi}_1^0}$. We start with the case-L, where we chose $m_{\tilde{l}_L} \sim M_1$, i.e. the left-handed charged sleptons as well as the sneutrinos are close in mass to the LSP. As analyzed in Refs. [8,9], one finds that all six sleptons are close in mass and differ by less than ~ 50 GeV.

In the upper plot of Fig. 4 we show the results of our scan in the $m_{\tilde{\chi}_1^0}$–Δm plane (with $\Delta m = m_{\tilde{\mu}_1} - m_{\tilde{\chi}_1^0}$). The color coding indicates the DM relic density, where the red points correspond to full agreement with the Planck measurement, see Eq. (4). The magenta points shown in the inlay are found below the neutrino floor, see below, where the solid line indicates the overall allowed parameter space. By definition of $\tilde{l}^{\pm}$-coannihilation the points are found for relatively low Δm, with mass differences between ~ 10 GeV and ~ 80 GeV.

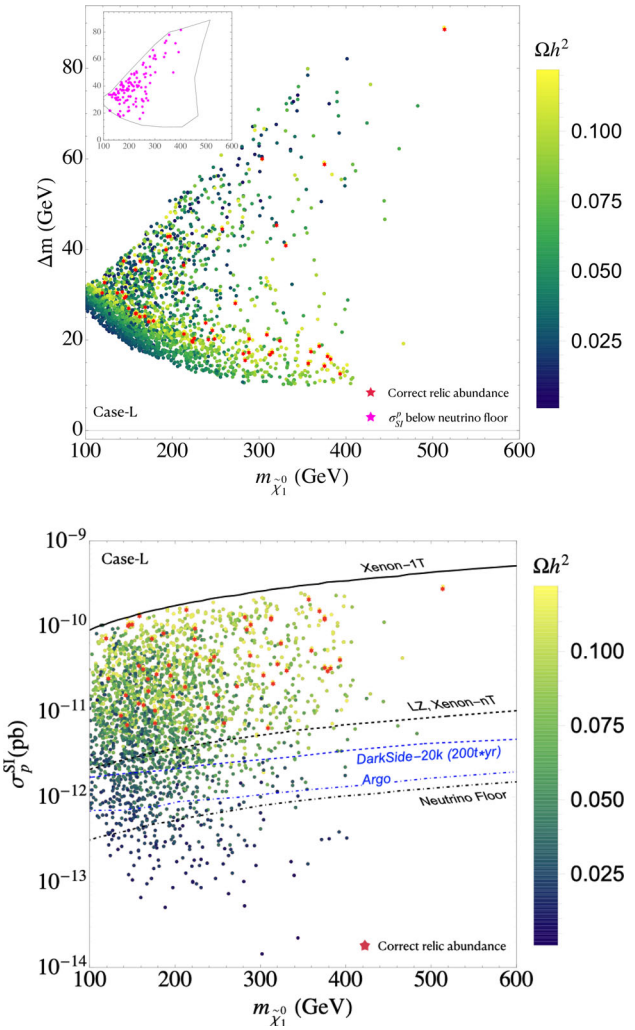

Fig. 4 The results of our parameter scan in the bino DM scenario with $\tilde{l}^{\pm}$-coannihilation case-L. Upper plot: $m_{\tilde{\chi}_1^0}$–Δm plane ($\Delta m = m_{\tilde{\mu}_1} - m_{\tilde{\chi}_1^0}$). Lower plot: $m_{\tilde{\chi}_1^0}$–$\sigma_p^{\rm SI}$ plane. The color code indicates the DM relic density. Red points are in full agreement with the Planck measurement. The magenta points shown in the inlay in the upper plot indicate the points below the neutrino floor, where the solid line indicates the overall allowed parameter space

For each $m_{\tilde{\chi}_1^0}$ the smallest achievable Δm values result in an underabundance of DM. Apart from that, no clear pattern can be observed for the location of the red points (fulfilling exactly the Planck measurements). Concerning the magenta points (below the neutrino floor) they are found only for $m_{\tilde{\chi}_1^0} \lesssim 400$ GeV, i.e. making them potentially easier to access at future collider experiments. In Sect. 6.1 we will discuss in more detail how the various population of points may be tested at the (HL-)LHC or a future e^+e^- collider.

The prediction for the DD experiments is presented in the lower plot of Fig. 4. We show the $m_{\tilde{\chi}_1^0}$–$\sigma_p^{\rm SI}$ plane, again with the color coding indicating the DM relic density. As in the previous cases, for the points with a lower relic density we rescale the cross-section with a factor of $(\Omega_{\tilde{\chi}} h^2/0.118)$

to take into account the fact that $\tilde{\chi}_1^0$ provides only a fraction of the total DM relic density of the universe. By construction, the upper limit of the points is provided by the XENON-1T limit. The red points, i.e. the ones in full agreement with the Planck measurement, are all above the future XENON-nT/LZ limit, i.e. the can all be tested in future DD experiments. This also holds for DarkSide (blue dashed) and Argo (blue dot-dashed), which have an even higher anticipated sensitivity. However, going to lower relic densities, on can observe that very low cross sections are reached for the lowest values of $\Omega_{\tilde{\chi}} h^2$. Those points can reach even values substantially below the neutrino floor, i.e. the prospects to cover them in DD experiments are currently unclear. On the other hand, as can be seen in the upper plot of Fig. 4, these points (indicated by magenta stars in the inlay) do not exceed $m_{\tilde{\chi}_1^0} \sim 500$ GeV. Their discovery prospects at the HL-LHC and future e^+e^- colliders with $\sqrt{s} = 1000$ GeV, i.e. the complementarity of DD and collider experiments will be discussed in Sect. 6.

5.5 Bino DM with $\tilde{l}^{\pm}$-coannihilation case-R

We now turn to our fifth scenario, bino DM with $\tilde{l}^{\pm}$-coannihilation case-R, where in the scan we require the "right-handed" sleptons to be close in mass with the LSP. Here it should be kept in mind that in our notation we do not mass-order the sleptons: for negligible mixing as it is given for selectrons and smuons the "left-handed" ("right-handed") slepton corresponds to $\tilde{l}_1$ ($\tilde{l}_2$). As discussed in Refs. [8,9], in this scenario all relevant mass scales are required to be relatively light by the $(g-2)_\mu$ constraint.

In the upper plot of Fig. 5 we show the results of our scan in the $m_{\tilde{\chi}_1^0}$–Δm plane (with $\Delta m = m_{\tilde{\mu}_2} - m_{\tilde{\chi}_1^0}$). The color coding indicates the DM relic density, where the red points correspond to full agreement with the Planck measurement, see Eq. (4). The (three) magenta points shown in the inlay are found below the neutrino floor, see below, where the solid line indicates the overall allowed parameter space. By definition of $\tilde{l}^{\pm}$-coannihilation the points are found for relatively low Δm. Contrary to case-L the red points (fulfilling exactly the Planck measurements) are distributed over the whole allowed parameter space. The sparse magenta points (below the neutrino floor, see below) are found between ~ 200 GeV $\lesssim m_{\tilde{\chi}_1^0} \lesssim 350$ GeV. In Sect. 6.1 we will discuss in more detail how the various population of points may be tested at the (HL-)LHC or a future e^+e^- collider.

The prediction for the DD experiments is presented in the lower plot of Fig. 5. We show the $m_{\tilde{\chi}_1^0}$–$\sigma_p^{\rm SI}$ plane, again with the color coding indicating the DM relic density. As before, for the points with a lower relic density we rescale the cross-section with a factor of $(\Omega_{\tilde{\chi}} h^2/0.118)$ to take into account the fact that $\tilde{\chi}_1^0$ provides only a fraction of the total DM relic density of the universe. By construction, the upper limit of the points is provided by the XENON-1T limit. The red points, i.e. the ones in full agreement with the Planck measurement, spread out substantially below the current XENON-1T limit. However, they do not go below the future anticipated XENON-nT/LZ limit (black dashed line), i.e. they can be covered by future DD experiments. This also holds for DarkSide (blue dashed) and Argo (blue dot-dashed), which have an even higher anticipated sensitivity.

Going to lower relic densities, one can observe that, as in the previously analyzed cases, very low cross sections are reached for the lowest values of $\Omega_{\tilde{\chi}} h^2$. Those points can reach even values going down to the neutrino floor, with three of them even below. It should be noted here that these three

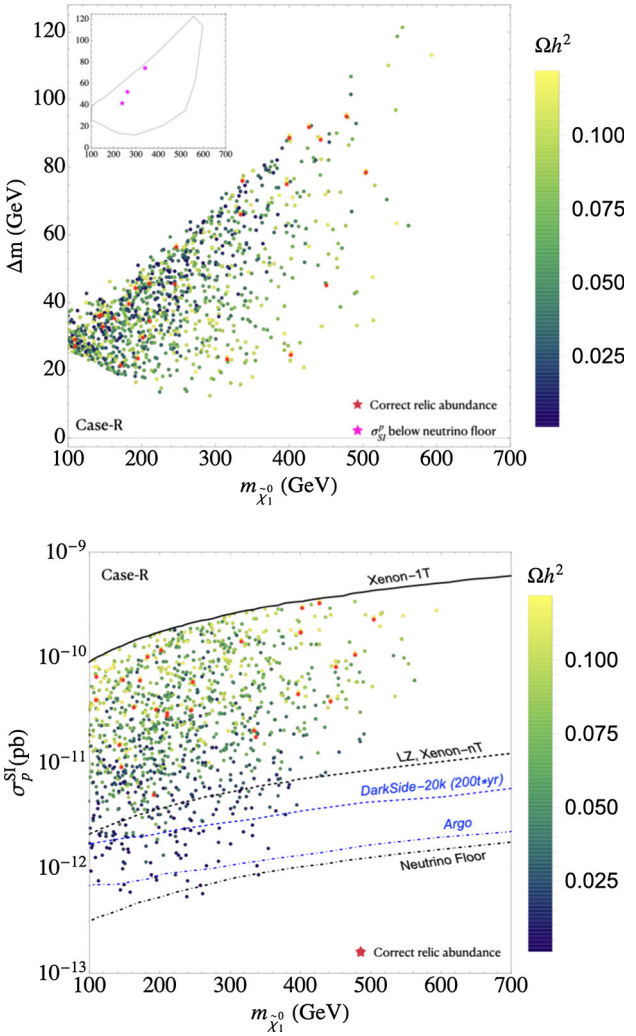

Fig. 5 The results of our parameter scan in the bino DM scenario with $\tilde{l}^{\pm}$-coannihilation case-R. Upper plot: $m_{\tilde{\chi}_1^0}$–Δm ($\Delta m = m_{\tilde{\mu}_2} - m_{\tilde{\chi}_1^0}$). Lower plot: $m_{\tilde{\chi}_1^0}$–$\sigma_p^{\rm SI}$ plane. The color code indicates the DM relic density. Red points are in full agreement with the Planck measurement. The magenta points shown in the inlay in the upper plot indicate the points below the neutrino floor, where the solid line indicates the overall allowed parameter space

points (marked as magenta stars in the upper inlay) are just on the border of the neutrino floor, which may be subject to some uncertainties [137]. Consequently, no firm conclusion can be drawn for them. On the other hand, as can be seen in the upper plot of Fig. 5, all points below the XENON-nT/LZ limit do not exceed $m_{\tilde{\chi}_1^0} \sim 400$ GeV. This leads to possibly very good prospects for their discovery at the HL-LHC or a future e^+e^- colliders with $\sqrt{s} = 1000$ GeV. The corresponding complementarity of DD and collider experiments will be discussed in the next section.

6 Complementarity with future collider experiments

In this section we analyze the complementarity between future DD experiments and searches at colliders. We concentrate on the parameter points that are below the anticipated limits of XENON-nT and LZ, and in particular on the points below the neutrino floor. We first show the prospects for searches for EW SUSY particles at the approved HL-LHC [138] and then at possible future high-energy e^+e^- colliders, such as the ILC [139,140] or CLIC [140–143].

6.1 HL-LHC prospects

The prospects for BSM phenomenology at the HL-LHC have been summarized in Ref. [138] for a 14 TeV run with 3 ab^{-1} of integrated luminosity per detector. For the wino, higgsino and bino/wino with $\tilde{\chi}_1^{\pm}$-coannihilation DM scenarios, the most relevant constraints may be derived either by searches specially designed to look for compressed spectra with low mass-splitting between $\tilde{\chi}_1^{\pm}$, $\tilde{\chi}_2^0$ and $\tilde{\chi}_1^0$, or complementary by searching for slepton pair-production at the HL-LHC. The projected discovery and 95% confidence level (C.L.) exclusion regions for the former search have been published by both CMS and ATLAS collaborations for the higgsino simplified model scenario. A naive application of the projected exclusion contours on our model parameter space (i.e. not taking into account the variation due to the difference in production cross section) shows that the higgsino and bino/wino scenarios will be covered in part by the HL-LHC, see, e.g., Fig. 22 in Ref. [9]. However, for the wino scenario the mass-splitting is too low to be probed by the compressed spectra searches. However, in this case, the improved HL-LHC sensitivity to disappearing track searches can prove to be useful, particularly in the region of very low mass-splittings [9]. For $\Delta m \sim 170$ MeV, the HL-LHC can probe wino masses up to about 900 GeV and 500 GeV at the 95% C.L., for the optimistic and conservative background estimations respectively.

So far, similar future sensitivity estimates for the slepton pair production searches by the experimental collaborations are lacking. However, in order to provide an estimate of the production cross section at the HL-LHC, we compute the NLO+NLL threshold resummed cross sections for $\tilde{e}_L^{\pm}\tilde{e}_L^{\mp}$ and $\tilde{\mu}_L^{\pm}\tilde{\mu}_L^{\mp}$ pair productions for the bino/wino DM scenario with $\tilde{\chi}_1^{\pm}$-coannihilation, using the public package Resummino [144–148]. The result is presented in Fig. 6, where in the upper left plot the production cross section is presented as a function of the mass difference between the produced particle and the LSP, $\Delta m = m_{\tilde{l}_L} - m_{\tilde{\chi}_1^0}$, and in the right plot it is shown as a function of $m_{\tilde{l}_L}$. The parameter points below the reach of XENON-nT/LZ are shown as green squares and those below the neutrino floor are marked with blue stars. The production proceeds through the s-channel exchange of Z bosons and photons. The cross-section for low $m_{\tilde{l}_L}$, also roughly corresponding to a low Δm, appear to be significantly large at the level of ~ 10 fb. However, here it must be taken into account that in this case, due to the proximity of $m_{\tilde{\chi}_1^{\pm}}$ and $m_{\tilde{\chi}_1^0}$, the sleptons have a significant BR($\tilde{l}^{\pm} \to \nu\tilde{\chi}_1^{\pm}$), as opposed to the simplified model assumption of BR($\tilde{l}^{\pm} \to l\tilde{\chi}_1^0$) = 100% . This reduces the effective cross section to a large extent, making the sleptons harder to be probed at the HL-LHC. Consequently, the complementarity between the DD experiments and the HL-LHC can not conclusively be answered.

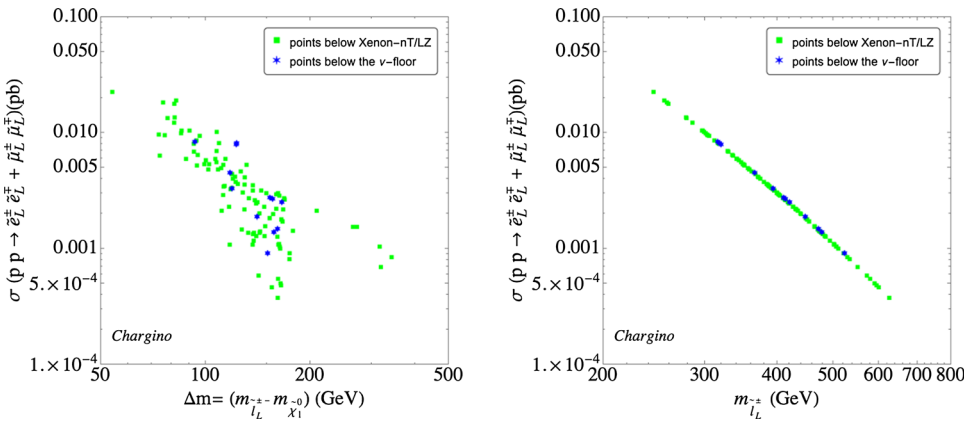

Fig. 6 Cross section predictions at $pp-$ collider with $\sqrt{s} = 14$ TeV as a function of the difference of two final state masses. for the $\tilde{\chi}_1^{\pm}$-coannihilation scenario. The color code indicates the final state, squares are below the anticipated XENON-nT/LZ reach, stars are below the neutrino floor

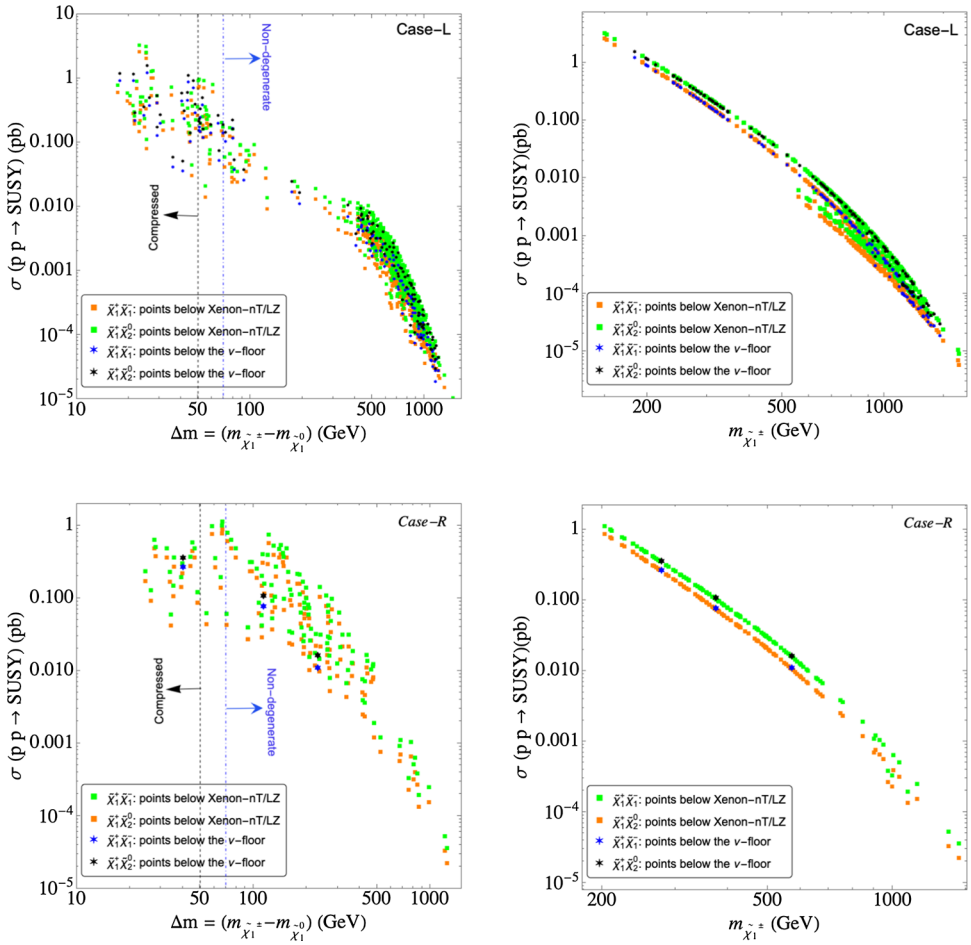

Fig. 7 Cross section predictions at $pp-$ collider with $\sqrt{s} = 14$ TeV as a function of $\Delta m = m_{\tilde{\chi}_1^\pm} - m_{\tilde{\chi}_1^0}$ (left) and $m_{\tilde{\chi}_1^\pm}$ (right). Upper row: $\tilde{l}^\pm$-coannihilation case-L; lower row: $\tilde{l}^\pm$-coannihilation case-R. The color code indicates the final state, squares are below the anticipated XENON-nT/LZ reach, stars are below the neutrino floor

For the bino DM scenario with $\tilde{l}^\pm$-coannihilation, the searches that could be the most constraining are those coming from compressed spectra searches looking for $\tilde{l}^\pm$-pair production, as well as the $\tilde{\chi}_1^\pm - \tilde{\chi}_2^0$ production searches leading to three leptons and $\not{E}_T$ in the final state. No projected sensitivity for the former search exists so far to our knowledge. For the latter search, the projected 95% C.L. exclusion contours have been provided by the ATLAS collaboration [138] for the decays $\tilde{\chi}_1^\pm\tilde{\chi}_2^0 \to W^\pm Z$ and $\tilde{\chi}_1^\pm\tilde{\chi}_2^0 \to W^\pm h$. The limits are given for simplified model scenarios assuming $\tilde{\chi}_1^\pm$ and $\tilde{\chi}_2^0$ to be purely wino-like and mass-degenerate and $\tilde{\chi}_1^0$ to be purely bino-like. These searches are most effective in the large mass splitting regions, $\Delta m = m_{\tilde{\chi}_1^\pm} - m_{\tilde{\chi}_1^0} \gtrsim M_Z$ and $\Delta m \gtrsim M_h$ for the $W^\pm Z$ and $W^\pm h$ modes, respectively, where they can probe masses up to $m_{\tilde{\chi}_1^\pm} = m_{\tilde{\chi}_2^0} \sim 1.2$ TeV. The parameter region where $m_{\tilde{\chi}_1^\pm}, m_{\tilde{\chi}_2^0} > m_{\tilde{l}_L}, m_{\tilde{l}_R}$, the $\tilde{\chi}_1^\pm$, $\tilde{\chi}_2^0$ may also decay via sleptons of the first two generations. The prospect for such decay channels, however has not been analyzed. In Fig. 7 we show our results for the relevant gaugino-pair production cross sections in the bino DM with $\tilde{l}^\pm$-coannihilation scenarios case-L (top row) and case-R (bottom row) derived at the NLO+NLL accuracy using Resummino. The squares and stars represent points below the sensitivity of XENON-nT/LZ and the neutrino floor, respectively. In the left plots we show the cross sections with respect to the mass difference $\Delta m = m_{\tilde{\chi}_1^\pm} - m_{\tilde{\chi}_1^0}$, indicating the regions corresponding to compressed and non-degenerate spectra. In the right plots the cross sections are shown as a function of $m_{\tilde{\chi}_1^\pm}$ directly. As in the case of $\tilde{\chi}_1^\pm$-coannihilation, the squarks are assumed to be very heavy in this case. Thus, the dominant production processes occur via the s-channel exchange of W, Z bosons and photons. The larger cross section in the low Δm regions may be beneficial for compressed spectra searches looking for $\tilde{\chi}_1^\pm - \tilde{\chi}_2^0$ pair production. In the higher Δm region, the cross section decreases steadily up to $m_{\tilde{\chi}_1^\pm} \sim 1.2$ TeV. As in the previous case, also here the apparently large cross section reached for relatively light $\tilde{\chi}_1^\pm$ should be interpreted with caution in deriving future exclusion/discovery potentials: on the one hand, $\tilde{\chi}_1^\pm$, $\tilde{\chi}_2^0$ may decay partly via sleptons of the first two generations, weakening the limits from gauge-boson or Higgs-mediated decays. On the other hand, they may decay to some extent via $\tilde{\tau}$'s, relaxing the bounds from both slepton-mediated and gauge/Higgs-boson mediated decays. As before, the complementarity between the

DD experiments and the HL-LHC can not conclusively be answered.

For the sake of completeness, we also show the production cross-section for the NLSPs in all three cases in Fig. 8 as a function of $\Delta m (= m_{\rm NLSP} - m_{\tilde{\chi}_1^0})$ as well as a function of $m_{\rm NLSP}$. The production cross-section at 14 TeV at NLO+NLL is the largest for the chargino co-annihilation reaching up to $\mathcal{O}(1\,\text{pb})$ for the minimum mass gap between the NLSP and LSP, while for case-L and case-R, it remains at least one order below. These pair production of chargino or slepton NLSPs corresponds to the compressed spectra searches at the HL-LHC where the final state signal comprises of ISR jets plus missing energy. However, future linear colliders will have better sensitivity to probe these signal regions. The details are discussed in the following section.

6.2 ILC/CLIC prospects

Direct production of EW particles at e^+e^- colliders requires a sufficiently high center-of-mass energy, $\sqrt{s}$. Consequently, we focus here on the two proposals for linear e^+e^- colliders, ILC [139,140] and CLIC [140–143], which can reach energies up to 1 TeV, and 3 TeV, respectively. The former one we also denote as ILC1000. We evaluate the cross-sections for the various LSP and NLSP pair production modes for $\sqrt{s} = 1$ TeV, which can be reached in the final stage of the ILC or are below the anticipated CLIC energies (where at higher $\sqrt{s}$ larger cross sections are obtained). At the ILC1000 an integrated luminosity of 8 ab^{-1} is foreseen [149,150]. The cross-section predictions are based on tree-level results, obtained as in Refs. [124,151]. There it was shown that the

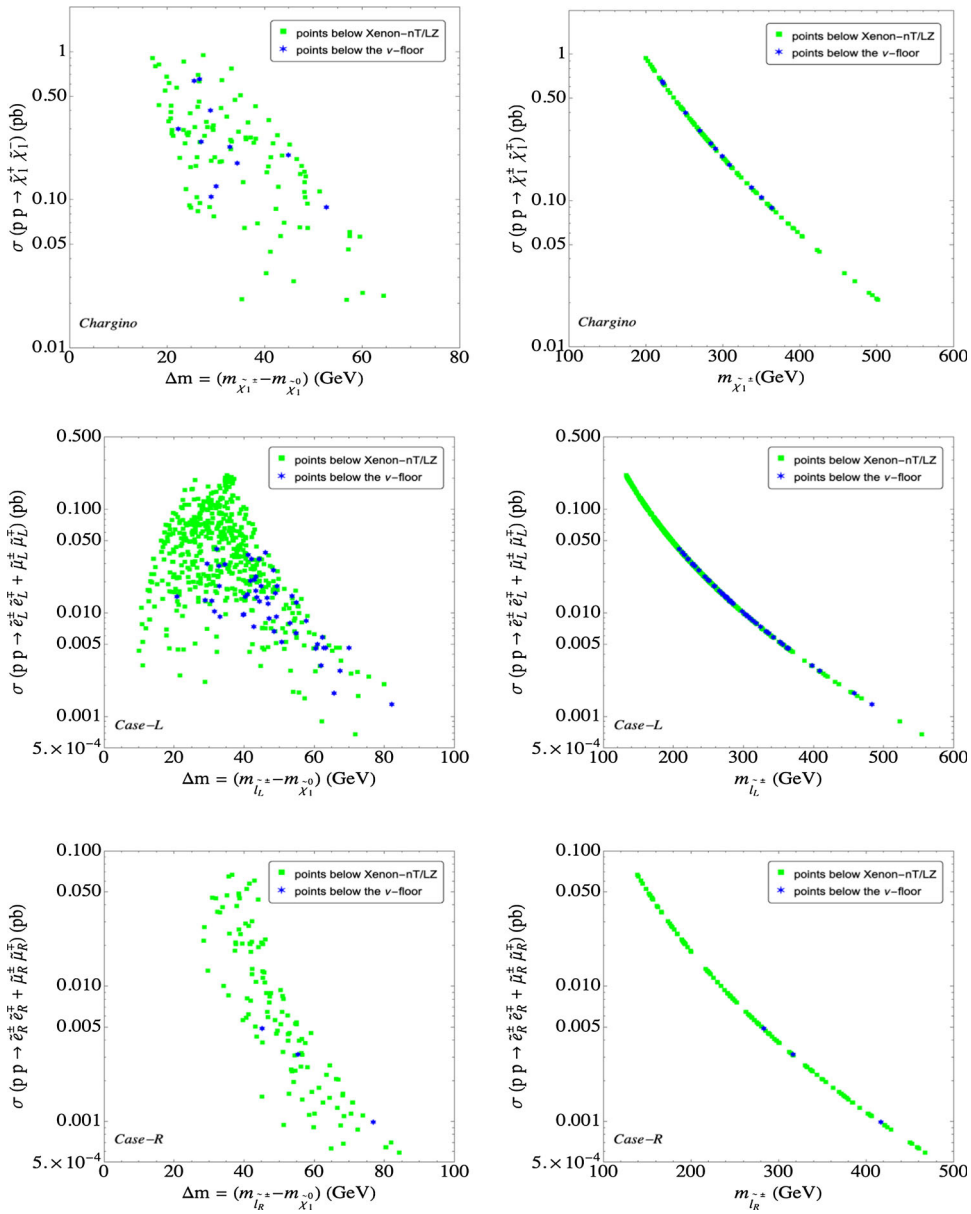

Fig. 8 Cross section predictions at $pp-$ collider with $\sqrt{s} = 14$ TeV as a function of $\Delta m = m_{\rm NLSP} - m_{\tilde{\chi}_1^0}$ (left) and $m_{\rm NLSP}$ - $m_{\tilde{\chi}_1^0}$ (right) for chargino (top), case-L (middle) and case-R(bottom). Green squares are below the anticipated XENON-nT/LZ reach and blue stars are below the neutrino floor

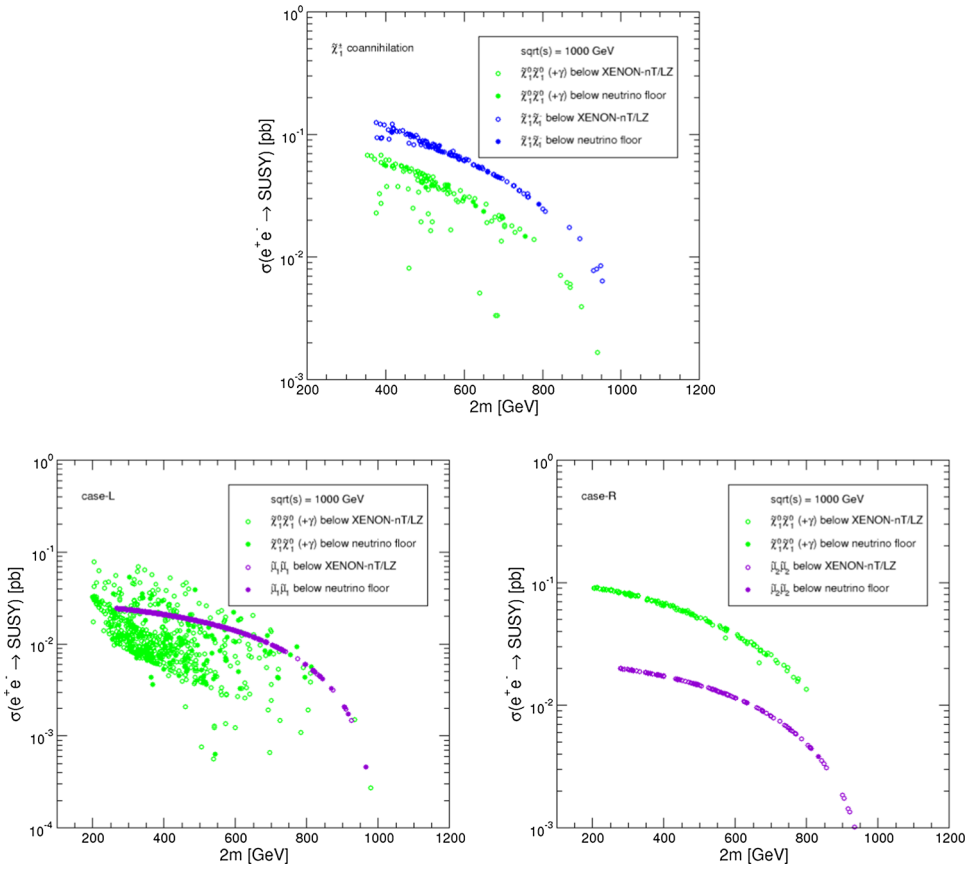

Fig. 9 Cross section predictions at an e^+e^- collider with $\sqrt{s} = 1000$ GeV as a function of the sum of two final state masses. Upper plot: $\tilde{\chi}_1^\pm$-coannihilation scenario; lower left plot: $\tilde{l}^\pm$-coannihilation case-L; lower right plot: $\tilde{l}^\pm$-coannihilation case-R. The color code indicates the final state, open circles are below the anticipated XENON-nT/LZ reach, full circles are below the neutrino floor

full one-loop corrections can amount up to 10-20% [5] . Here we do not attempt a rigorous experimental analysis, but follow analyses [152–154] that indicate that to a good approximation final states with the sum of the masses smaller than the center-of-mass energy can be detected.

In Fig. 9 we show the LSP and NLSP pair production cross sections for an e^+e^- collider at $\sqrt{s} = 1000$ GeV as a function of the two (identical) final state masses. The upper plot shows $\sigma(e^+e^- \to \tilde{\chi}_1^0\tilde{\chi}_1^0(+\gamma))$ production [6] in green, and $\sigma(e^+e^- \to \tilde{\chi}_1^+\tilde{\chi}_1^-)$ in blue. The open circles are the points below the anticipated XENON-nT/LZ limit, whereas the solid circles are the points below the neutrino floor. On can observe that *all* points are within the reach of the ILC1000. The cross sections range roughly from $\sim$ 100 fb for low masses to $\sim$ 10 fb for larger masses, with only a very few points have smaller cross sections. Overall, assuming an integrated luminosity of 8 ab^{-1}, this corresponds to $\sim 80000 - 800000$ events. Consequently, in contrast to the HL-LHC, the e^+e^- colliders show a clear and conclusive complementarity to the future DD experiments. The $\tilde{\chi}_1^\pm$-coannihilation scenario will be fully covered by either DD experiments or by searches at the ILC1000.

The lower plots of Fig. 9 show the LSP and NLSP production cross section in the $\tilde{l}^\pm$-coannihilation scenario for case-L (left) and case-R (right). The green points show again $\sigma(e^+e^- \to \tilde{\chi}_1^0\tilde{\chi}_1^0(+\gamma))$, whereas the violet points left and right show $\sigma(e^+e^- \to \tilde{\mu}_1\tilde{\mu}_1)$ (case-L) and $\sigma(e^+e^- \to \tilde{\mu}_2\tilde{\mu}_2)$ (case-R), respectively. Open and full circles denote, as above, the points below the anticipated XENON-nT/LZ limit and the neutrino floor. The visible spread in the $\tilde{\chi}_1^0\tilde{\chi}_1^0(+\gamma)$ production for case-L w.r.t. case-R is a result of the more complex structure of the $e^\pm$-$\tilde{e}_L$-$\tilde{\chi}_1^0$ coupling as compared to the $e^\pm$-$\tilde{e}_R$-$\tilde{\chi}_1^0$ coupling, dominating the t-channel exchange diagram, respectively. In both cases we see that, as for the $\tilde{\chi}_1^\pm$-coannihilation case, all points result in particles that can be pair produced at the ILC1000 (except the very highest mass points in case-L). The cross sections range between 100 fb to 10 fb for $\tilde{\chi}_1^0\tilde{\chi}_1^0(+\gamma)$, and between 20 fb to 1 fb for smuon pair production. Even for the smallest production cross section this corresponds to $\sim$ 8000 events in the foreseen 1000 GeV ILC run. Also these two cases can conclusively be probed

[5] Including the full one-loop corrections here as done in Refs. [124, 151] would have required to determine the preferred renormalization scheme for each point individually (see Ref. [123] for details), which goes beyond the scope of this analysis.

[6] Our tree level calculation does not include the photon radiation, which appears only starting from the one-loop level. However, such an ISR photon is crucial to detect this process due to the invisible final state. We take our tree-level cross section as a rough approximation of the cross section including the ISR photon, see also Ref. [124] and use the notation "$(+\gamma)$".

in the conjunction of DD experiments and an e^+e^- collider at $\sqrt{s} = 1000$ GeV, in contrast to the HL-LHC, where the prospects are less clear, see the previous subsection.

7 Conclusions

We performed an analysis for the DM predictions of the EW sector of the MSSM, taking into account all relevant theoretical and experimental constraints. The experimental results comprised the direct searches at the LHC, the current DM relic abundance (either as an upper limit or as a direct measurement), the DM direct detection (DD) experiments and in particular the newly confirmed deviation of the anomalous magnetic moment of the muon [17]. As we had analyzed previously [8–10], five different scenarios can be classified by the mechanism that brings the LSP relic density into agreement with the measured values. These are *(i)* higgsino DM ($\mu < M_1, M_2, m_{\tilde{l}_L}, m_{\tilde{l}_R}$), DM relic density is only an upper bound (the correct relic density implies $m_{\tilde{\chi}_1^0} \sim 1$ TeV and $(g-2)_\mu$ cannot be fulfilled), $m_{\text{(N)LSP}} \lesssim 500$ GeV with $m_{\text{NLSP}} - m_{\text{LSP}} \sim 5$ GeV; *(ii)* wino DM ($M_2 < M_1, \mu, m_{\tilde{l}_L}, m_{\tilde{l}_R}$), DM relic density is only an upper bound, (the correct relic abundance implies $m_{\tilde{\chi}_1^0} \sim 3$ TeV and $(g-2)_\mu$ cannot be fulfilled), $m_{\text{(N)LSP}} \lesssim 600$ GeV with $m_{\text{NLSP}} - m_{\text{LSP}} \sim 0.3$ GeV. *(iii)* bino/wino DM with $\tilde{\chi}_1^\pm$-coannihilation ($M_1 \lesssim M_2$), correct DM relic density can be achieved, $m_{\text{(N)LSP}} \lesssim 650\,(700)$ GeV; *(iv)* bino DM with $\tilde{l}^\pm$-coannihilation case-L ($M_1 \lesssim m_{\tilde{l}_L}$), DM relic density can be fulfilled, $m_{\text{(N)LSP}} \lesssim 650\,(700)$ GeV; *(v)* bino DM with $\tilde{l}^\pm$-coannihilation case-R ($M_1 \lesssim m_{\tilde{l}_R}$), DM relic density can be fulfilled, $m_{\text{(N)LSP}} \lesssim 650\,(700)$ GeV;

In this letter we addressed the status of the implications of the new result for Δa_μ (in conjunction with the other constraints) for the DM predictions in the five scenarios. In a first step we analyzed the predictions for the DM relic density as a function of the (N)LSP masses. For higgsino and wino DM we analyzed the case where the $\tilde{\chi}_1^0$ satisfies only a part of the total DM content while being consistent with Δa_μ. On the contrary, for bino/wino DM and the two bino DM cases, the $\tilde{\chi}_1^0$ LSP can yield the total DM relic abundance, or only a part of the total DM content (with the relic abundance limit taken as an upper bound). As evident, for the heavier mass region of the LSP, significant coannihilation is necessary to achieve the relic abundance leading to the smallest mass gap between the NLSP and LSP for all these cases. However, for higgsino and wino DM, the NLSP-LSP mass gap is inherently smaller than the other three cases that results in a much compressed spectra.

In a second step we evaluated the prospects for future DD experiments in the five scenarios. We observed that higgsino and wino DM can be covered by the "next round of DM DD experiments", where we showed explicitly the anticipated reach of XENON-nT, LZ, DarkSide and Argo. XENON-nT and LZ have a similar reach, which is moderately improved by DarkSide and a little more by Argo. For higgsino and wino DM all allowed points are well in the reach of XENON-nT/LZ. Therefore, besides the compressed spectra searches at the future hadron and lepton collider, the future DD experiments are also capable of testing these scenarios conclusively. For slepton coannihilation case-L and case-R, the allowed points with the correct relic abundance are above the projected reach of XENON-nT/LZ, whereas for bino/wino DM with chargino coannihilation a few points also fall within the higher anticipated sensitivity of DarkSide. For lower relic abundances the σ_p^{SI} values decrease further for these three scenarios and can go even below the neutrino floor. However, in the case of bino case-R DM, the points with the lowest σ_p^{SI} are found only marginally below the neutrino floor and thus can potentially be covered by further future DD experiments.

In continuation, we show that the HL-LHC and the future e^+e^- collider operating at an energy of up to 1000 GeV, i.e. the ILC1000 or CLIC can play the complementary role to probe the parameter space obtained below the anticipated XENON-nT/LZ limit or even below the neutrino floor. For the HL-LHC we focused on the production of the EW particles which are neither the LSP nor the NLSP, i.e. that are not necessarily part of a compressed EW spectrum. While partially sizable cross sections are found at the HL-LHC with $\sqrt{s} = 14$ TeV, in particular in the lower mass ranges, a proper estimation of the future reach including the complex decay structure of the signal region is mandatory (which often so far are not available) to make a conclusive judgement. On the other hand, in the higher mass range, the EW SUSY production cross sections sharply drops below fb order, specifically for $\tilde{l}^\pm$-coannihilation. Consequently, it appears unlikely that the points that may escape the DD experiments can fully be probed at the HL-LHC. For completeness we also calculated the production cross-sections for the compressed spectra searches at the HL-LHC, where again detailed analyses are not yet available.

The situation is substantially better in the case of an e^+e^- collider with $\sqrt{s} \lesssim 1$ TeV. It was shown that at the ILC or CLIC mass spectra with very small mass splitting can be detected, i.e. one does not have to rely on the production of heavier SUSY particles, but can study the production of the LSP (with an ISR photon) and the NLSP. We have calculated the corresponding production cross sections for all points below the XENON-nT/LZ limit or the neutrino floor. It was shown that effectively the whole parameter space that may escape the DD experiments can be covered by ILC1000/CLIC. This demonstrates the important complementarity of DD experiments and future (linear) e^+e^- colliders to cover the EW sector of the MSSM.

Acknowledgements We thank D. Cerdeño and G. Moortgat-Pick for helpful discussions. I.S. thanks S. Matsumoto for the cluster facility. The work of I.S. is supported by World Premier International Research Center Initiative (WPI), MEXT, Japan. The work of S.H. is supported in part by the MEINCOP Spain under contract PID2019-110058GB-C21 and in part by the AEI through the grant IFT Centro de Excelencia Severo Ochoa SEV-2016-0597. The work of M.C. is supported by the project AstroCeNT: Particle Astrophysics Science and Technology Centre, carried out within the International Research Agendas programme of the Foundation for Polish Science financed by the European Union under the European Regional Development Fund.

Data Availability Statement This manuscript has no associated data or the data will not be deposited. [Authors' comment: There is no additional data or the data is already included in the manuscript.]

Funded by SCOAP[3].

References

1. H. Nilles, Phys. Rep. **110**, 1 (1984)
2. R. Barbieri, Riv. Nuovo Cim. **11**, 1 (1988)
3. H. Haber, G. Kane, Phys. Rep. **117**, 75 (1985)
4. J. Gunion, H. Haber, Nucl. Phys. B **272**, 1 (1986)
5. H. Goldberg, Phys. Rev. Lett. **50**, 1419 (1983)
6. J. Ellis, J. Hagelin, D. Nanopoulos, K. Olive, M. Srednicki, Nucl. Phys. B **238**, 453 (1984)
7. K.J. Bae, H. Baer, E.J. Chun, Phys. Rev. D **89**(3), 031701 (2014). arXiv:1309.0519 [hep-ph]
8. M. Chakraborti, S. Heinemeyer, I. Saha, Eur. Phys. J. **C 80**(10), 984 (2020). arXiv:2006.15157 [hep-ph]
9. M. Chakraborti, S. Heinemeyer, I. Saha, Eur. Phys. J. **C 81**(12), 1069 (2021). arXiv:2103.13403 [hep-ph]
10. M. Chakraborti, S. Heinemeyer, I. Saha, Eur. Phys. J. **C 81**(12), 1114 (2021). arXiv:2104.03287 [hep-ph]
11. See: https://twiki.cern.ch/twiki/bin/view/AtlasPublic/SupersymmetryPublicResults. Accessed 24 May 2022
12. See: https://twiki.cern.ch/twiki/bin/view/CMSPublic/PhysicsResultsSUS. Accessed 24 May 2022
13. N. Aghanim et al. (Planck Collaboration), Astron. Astrophys. **641**, A6 (2020). arXiv:1807.06209 [astro-ph.CO] [Erratum: Astron. Astrophys. **652**, C4 (2021)]
14. E. Aprile et al. (XENON Collaboration), Phys. Rev. Lett. **121**(11), 111302 (2018). arXiv:1805.12562 [astro-ph.CO]
15. D.S. Akerib et al. (LUX Collaboration), Phys. Rev. Lett. **118**(2), 021303 (2017). arXiv:1608.07648 [astro-ph.CO]
16. X. Cui et al. (PandaX-II Collaboration), Phys. Rev. Lett. **119**(18), 181302 (2017). arXiv:1708.06917 [astro-ph.CO]
17. B. Abi et al. (Muon g-2), Phys. Rev. Lett. **126**(14), 141801 (2021). arXiv:2104.03281 [hep-ex]
18. G.W. Bennett et al. (Muon g-2 Collaboration), Phys. Rev. D **73**, 072003 (2006). arXiv:hep-ex/0602035
19. M. Endo, K. Hamaguchi, S. Iwamoto, T. Kitahara, JHEP **07**, 075 (2021). arXiv:2104.03217 [hep-ph]
20. S. Iwamoto, T.T. Yanagida, N. Yokozaki, Phys. Lett. B **823**, 136768 (2021). arXiv:2104.03223 [hep-ph]
21. Y. Gu, N. Liu, L. Su, D. Wang, Nucl. Phys. B **969**, 115481 (2021). arXiv:2104.03239 [hep-ph]
22. M. Van Beekveld, W. Beenakker, M. Schutten, J. De Wit, SciPost Phys. **11**, 049 (2021). arXiv:2104.03245 [hep-ph]
23. W. Yin, JHEP **06**, 029 (2021). arXiv:2104.03259 [hep-ph]
24. F. Wang, L. Wu, Y. Xiao, J.M. Yang, Y. Zhang, Nucl. Phys. B **970**, 115486 (2021). arXiv:2104.03262 [hep-ph]
25. M. Abdughani, Y.Z. Fan, L. Feng, Y.L. Sming Tsai, L. Wu, Q. Yuan, Sci. Bull. **66**, 2170–2174 (2021). arXiv:2104.03274 [hep-ph]
26. J. Cao, J. Lian, Y. Pan, D. Zhang, P. Zhu, JHEP **09**, 175 (2021). arXiv:2104.03284 [hep-ph]
27. M. Ibe, S. Kobayashi, Y. Nakayama, S. Shirai, JHEP **07**, 098 (2021). arXiv:2104.03289 [hep-ph]
28. P. Cox, C. Han, T.T. Yanagida, Phys. Rev. D **104**(7), 075035 (2021). arXiv:2104.03290 [hep-ph]
29. C. Han, arXiv:2104.03292 [hep-ph]
30. S. Heinemeyer, E. Kpatcha, I. Lara, D.E. López-Fogliani, C. Muñoz, N. Nagata, Eur. Phys. J. C **81**(9), 802 (2021). arXiv:2104.03294 [hep-ph]
31. S. Baum, M. Carena, N.R. Shah, C.E.M. Wagner, JHEP **01**, 025 (2022), arXiv:2104.03302 [hep-ph]
32. H.B. Zhang, C.X. Liu, J.L. Yang, T.F. Feng, Chinese Physics C **46** (2022). arXiv:2104.03489 [hep-ph]
33. W. Ahmed, I. Khan, J. Li, T. Li, S. Raza, W. Zhang, Phys. Lett. B **827**, 136879 (2022). arXiv:2104.03491 [hep-ph]
34. P. Athron, C. Balázs, D.H. Jacob, W. Kotlarski, D. Stöckinger, H. Stöckinger-Kim, JHEP **09**, 080 (2021). arXiv:2104.03691 [hep-ph]
35. A. Aboubrahim, M. Klasen, P. Nath, Phys. Rev. D **104**(3), 035039 (2021). arXiv:2104.03839 [hep-ph]
36. M. Chakraborti, L. Roszkowski, S. Trojanowski, JHEP **05**, 252 (2021). arXiv:2104.04458 [hep-ph]
37. H. Baer, V. Barger, H. Serce, Phys. Lett. B **820**, 136480 (2021). arXiv:2104.07597 [hep-ph]
38. W. Altmannshofer, S.A. Gadam, S. Gori, N. Hamer, JHEP **07**, 118 (2021). arXiv:2104.08293 [hep-ph]
39. M. Chakraborti, S. Heinemeyer, I. Saha, arXiv:2105.06408 [hep-ph]
40. M.D. Zheng, H.H. Zhang, Phys. Rev. D **104**(11), 115023 (2021) arXiv:2105.06954 [hep-ph]
41. K.S. Jeong, J. Kawamura, C.B. Park, JHEP **10**, 064 (2021). arXiv:2106.04238 [hep-ph]
42. Z. Li, G.L. Liu, F. Wang, J.M. Yang, Y. Zhang, JHEP **12**, 219 (2021). arXiv:2106.04466 [hep-ph]
43. P.S.B. Dev, A. Soni, F. Xu, arXiv:2106.15647 [hep-ph]
44. J.S. Kim, D.E. Lopez-Fogliani, A.D. Perez, R.R. de Austri, Nucl. Phys. B **974**, 115637 (2022). arXiv:2107.02285 [hep-ph]
45. J. Ellis, J.L. Evans, N. Nagata, D.V. Nanopoulos, K.A. Olive, Eur. Phys. J. C **81**(12), 1079 (2021). arXiv:2107.03025 [hep-ph]
46. S.M. Zhao, L.H. Su, X.X. Dong, T.T. Wang, T.F. Feng, JHEP **03**, 101 (2022). arXiv:2107.03571 [hep-ph]
47. M. Frank, Y. Hiçyılmaz, S. Mondal, Ö. Özdal, C.S. Ün, JHEP **10**, 063 (2021). arXiv:2107.04116 [hep-ph]
48. Q. Shafi, C.S. Un, arXiv:2107.04563 [hep-ph]
49. S. Li, Y. Xiao, J.M. Yang, Eur. Phys. J. C **82**(3), 276 (2022). arXiv:2107.04962 [hep-ph]
50. A. Aranda, F.J. de Anda, A.P. Morais, R. Pasechnik, arXiv:2107.05495 [hep-ph]

51. A. Aboubrahim, M. Klasen, P. Nath, R.M. Syed, arXiv:2107.06021 [hep-ph]
52. Y. Nakai, M. Reece, M. Suzuki, JHEP **10**, 068 (2021). arXiv:2107.10268 [hep-ph]
53. T. Li, J.A. Maxin, D.V. Nanopoulos, Eur. Phys. J. C **81**(12), 1059 (2021). arXiv:2107.12843 [hep-ph]
54. S. Li, Y. Xiao, J.M. Yang, Nucl. Phys. B **974**, 115629 (2022). arXiv:2108.00359 [hep-ph]
55. J.L. Lamborn, T. Li, J.A. Maxin, D.V. Nanopoulos, JHEP **11**, 081 (2021). arXiv:2108.08084 [hep-ph]
56. O. Fischer, B. Mellado, S. Antusch, E. Bagnaschi, S. Banerjee, G. Beck, B. Belfatto, M. Bellis, Z. Berezhiani, M. Blanke et al. arXiv:2109.06065 [hep-ph]
57. A.K. Forster, S.F. King, Nucl. Phys. B **976**, 115700 (2022). arXiv:2109.10802 [hep-ph]
58. W. Ke, P. Slavich, Eur. Phys. J. C **82**(1), 89 (2022). arXiv:2109.15277 [hep-ph]
59. J. Ellis, J.L. Evans, N. Nagata, D.V. Nanopoulos, K.A. Olive, Eur. Phys. J. C **81**(12), 1109 (2021). arXiv:2110.06833 [hep-ph]
60. P. Athron, C. Balázs, D. Jacob, W. Kotlarski, D. Stöckinger, H. Stöckinger-Kim, PoS EPS-HEP2021 (2022) 695. arXiv:2110.07156 [hep-ph]
61. M. Chakraborti, S. Heinemeyer, I. Saha, PoS EPS-HEP2021 (2022) 694. arXiv:2111.00322 [hep-ph]
62. E. Bagnaschi et al., Eur. Phys. J. C **78**(3), 256 (2018). arXiv:1710.11091 [hep-ph]
63. P. Slavich, S. Heinemeyer (eds.), E. Bagnaschi et al., Eur. Phys. J. C **81**(5), 450 (2021). arXiv:2012.15629 [hep-ph]
64. T. Aoyama et al., Phys. Rep. **887**, 1–166 (2020). arXiv:2006.04822 [hep-ph]
65. T. Aoyama, M. Hayakawa, T. Kinoshita, M. Nio, Phys. Rev. Lett. **109**, 111808 (2012). arXiv:1205.5370 [hep-ph]
66. T. Aoyama, T. Kinoshita, M. Nio, Atoms **7**(1), 28 (2019)
67. A. Czarnecki, W.J. Marciano, A. Vainshtein, Phys. Rev. D **67**, 073006 (2003). arXiv:hep-ph/0212229
68. C. Gnendiger, D. Stöckinger, H. Stöckinger-Kim, Phys. Rev. D **88**, 053005 (2013). arXiv:1306.5546 [hep-ph]
69. M. Davier, A. Hoecker, B. Malaescu, Z. Zhang, Eur. Phys. J. C **77**(12), 827 (2017). arXiv:1706.09436 [hep-ph]
70. A. Keshavarzi, D. Nomura, T. Teubner, Phys. Rev. D **97**(11), 114025 (2018). arXiv:1802.02995 [hep-ph]
71. G. Colangelo, M. Hoferichter, P. Stoffer, JHEP **02**, 006 (2019). arXiv:1810.00007 [hep-ph]
72. M. Hoferichter, B.L. Hoid, B. Kubis, JHEP **08**, 137 (2019). arXiv:1907.01556 [hep-ph]
73. M. Davier, A. Hoecker, B. Malaescu, Z. Zhang, Eur. Phys. J. C **80**(3), 241 (2020). arXiv:1908.00921 [hep-ph] [Erratum: Eur. Phys. J. C **80**(5), 410 (2020)]
74. A. Keshavarzi, D. Nomura, T. Teubner, Phys. Rev. D **101**(1), 014029 (2020). arXiv:1911.00367 [hep-ph]
75. A. Kurz, T. Liu, P. Marquard, M. Steinhauser, Phys. Lett. B **734**, 144–147 (2014). arXiv:1403.6400 [hep-ph]
76. K. Melnikov, A. Vainshtein, Phys. Rev. D **70**, 113006 (2004). arXiv:hep-ph/0312226
77. P. Masjuan, P. Sanchez-Puertas, Phys. Rev. D **95**(5), 054026 (2017). arXiv:1701.05829 [hep-ph]
78. G. Colangelo, M. Hoferichter, M. Procura, P. Stoffer, JHEP **04**, 161 (2017). arXiv:1702.07347 [hep-ph]
79. M. Hoferichter, B.L. Hoid, B. Kubis, S. Leupold, S.P. Schneider, JHEP **10**, 141 (2018). arXiv:1808.04823 [hep-ph]
80. A. Gérardin, H.B. Meyer, A. Nyffeler, Phys. Rev. D **100**(3), 034520 (2019). arXiv:1903.09471 [hep-lat]
81. J. Bijnens, N. Hermansson-Truedsson, A. Rodríguez-Sánchez, Phys. Lett. B **798**, 134994 (2019). arXiv:1908.03331 [hep-ph]
82. G. Colangelo, F. Hagelstein, M. Hoferichter, L. Laub, P. Stoffer, JHEP **03**, 101 (2020). arXiv:1910.13432 [hep-ph]
83. T. Blum, N. Christ, M. Hayakawa, T. Izubuchi, L. Jin, C. Jung, C. Lehner, Phys. Rev. Lett. **124**(13), 132002 (2020). arXiv:1911.08123 [hep-lat]
84. G. Colangelo, M. Hoferichter, A. Nyffeler, M. Passera, P. Stoffer, Phys. Lett. B **735**, 90–91 (2014). arXiv:1403.7512 [hep-ph]
85. S. Borsanyi et al., Nature **593**(7857), 51–55 (2021). arXiv:2002.12347 [hep-lat]
86. C. Lehner, A.S. Meyer, Phys. Rev. D **101**, 074515 (2020). arXiv:2003.04177 [hep-lat]
87. A. Crivellin, M. Hoferichter, C.A. Manzari, M. Montull, Phys. Rev. Lett. **125**(9), 091801 (2020). arXiv:2003.04886 [hep-ph]
88. A. Keshavarzi, W.J. Marciano, M. Passera, A. Sirlin, Phys. Rev. D **102**(3), 033002 (2020). arXiv:2006.12666 [hep-ph]
89. E. de Rafael, Phys. Rev. D **102**(5), 056025 (2020). arXiv:2006.13880 [hep-ph]
90. P. Athron et al., Eur. Phys. J. C **76**(2), 62 (2016). arXiv:1510.08071 [hep-ph]
91. P. von Weitershausen, M. Schafer, H. Stöckinger-Kim, D. Stöckinger, Phys. Rev. D **81**, 093004 (2010). arXiv:1003.5820 [hep-ph]
92. H. Fargnoli, C. Gnendiger, S. Paßehr, D. Stöckinger, H. Stöckinger-Kim, JHEP **1402**, 070 (2014). arXiv:1311.1775 [hep-ph]
93. M. Bach, Jh. Park, D. Stöckinger, H. Stöckinger-Kim, JHEP **1510**, 026 (2015). arXiv:1504.05500 [hep-ph]
94. S. Heinemeyer, D. Stöckinger, G. Weiglein, Nucl. Phys. **B 690**, 62–80 (2004). arXiv:hep-ph/0312264
95. S. Heinemeyer, D. Stöckinger, G. Weiglein, Nucl. Phys. B **699**, 103–123 (2004). arXiv:hep-ph/0405255
96. W.G. Hollik, G. Weiglein, J. Wittbrodt, JHEP **03**, 109 (2019). arXiv:1812.04644 [hep-ph]
97. P.M. Ferreira, M. Mühlleitner, R. Santos, G. Weiglein, J. Wittbrodt, JHEP **09**, 006 (2019). arXiv:1905.10234 [hep-ph]
98. M. Drees, H. Dreiner, D. Schmeier, J. Tattersall, J.S. Kim, Comput. Phys. Commun. **187**, 227–265 (2015). arXiv:1312.2591 [hep-ph]
99. J.S. Kim, D. Schmeier, J. Tattersall, K. Rolbiecki, Comput. Phys. Commun. **196**, 535–562 (2015). arXiv:1503.01123 [hep-ph]
100. D. Dercks, N. Desai, J.S. Kim, K. Rolbiecki, J. Tattersall, T. Weber, Comput. Phys. Commun. **221**, 383–418 (2017). arXiv:1611.09856 [hep-ph]
101. M. Aaboud et al. (ATLAS Collaboration), Eur. Phys. J. C **78**(12), 995 (2018). arXiv:1803.02762 [hep-ex]
102. G. Aad et al. (ATLAS Collaboration), Eur. Phys. J. C **80**(2), 123 (2020). arXiv:1908.08215 [hep-ex]
103. G. Aad et al. (ATLAS Collaboration), Phys. Rev. D **101**(5), 052005 (2020). arXiv:1911.12606 [hep-ex]
104. M. Aaboud et al. (ATLAS Collaboration), JHEP **06**, 022 (2018). arXiv:1712.02118 [hep-ex]
105. A.M. Sirunyan et al. (CMS Collaboration), Phys. Lett. B **806**, 135502 (2020). arXiv:2004.05153 [hep-ex]
106. G. Belanger, F. Boudjema, A. Pukhov, A. Semenov, Comput. Phys. Commun. **149**, 103–120 (2002). arXiv:hep-ph/0112278
107. G. Belanger, F. Boudjema, A. Pukhov, A. Semenov, Comput. Phys. Commun. **176**, 367–382 (2007). arXiv:hep-ph/0607059
108. G. Belanger, F. Boudjema, A. Pukhov, A. Semenov, Comput. Phys. Commun. **177**, 894–895 (2007)
109. G. Belanger, F. Boudjema, A. Pukhov, A. Semenov, Comput. Phys. Commun. **185**, 960–985 (2014). arXiv:1305.0237 [hep-ph]
110. A. Sommerfeld, Ann. Phys. **403**, 257 (1931)
111. T.R. Slatyer, arXiv:1710.05137 [hep-ph]
112. A. Hryczuk, K. Jodlowski, E. Moulin, L. Rinchiuso, L. Roszkowski, E.M. Sessolo, S. Trojanowski, JHEP **10**, 043 (2019). arXiv:1905.00315 [hep-ph]

113. L. Rinchiuso, O. Macias, E. Moulin, N.L. Rodd, T.R. Slatyer, Phys. Rev. D **103**(2), 023011 (2021). arXiv:2008.00692 [astro-ph.HE]
114. R.T. Co, B. Sheff, J.D. Wells, Phys. Rev. D **105**(3), 035012 (2022). arXiv:2105.12142 [hep-ph]
115. H. Baer, V. Barger, P. Huang, A. Mustafayev, X. Tata, Phys. Rev. Lett. **109**, 161802 (2012). arXiv:1207.3343 [hep-ph]
116. H. Baer, V. Barger, D. Mickelson, Phys. Rev. D **88**(9), 095013 (2013). arXiv:1309.2984 [hep-ph]
117. H. Baer, V. Barger, M. Savoy, H. Serce, Phys. Lett. B **758**, 113–117 (2016). arXiv:1602.07697 [hep-ph]
118. H. Baer, V. Barger, D. Sengupta, X. Tata, Eur. Phys. J. C **78**(10), 838 (2018). arXiv:1803.11210 [hep-ph]
119. K.J. Bae, H. Baer, V. Barger, D. Sengupta, Phys. Rev. D **99**(11), 115027 (2019). arXiv:1902.10748 [hep-ph]
120. H. Baer, V. Barger, S. Salam, D. Sengupta, Phys. Rev. D **102**(7), 075012 (2020). arXiv:2005.13577 [hep-ph]
121. A. Delgado, M. Quirós, Phys. Rev. D **103**(1), 015024 (2021). arXiv:2008.00954 [hep-ph]
122. E. Bagnaschi et al., Eur. Phys. J. C **77**(4), 268 (2017). arXiv:1612.05210 [hep-ph]
123. T. Fritzsche, T. Hahn, S. Heinemeyer, F. von der Pahlen, H. Rzehak, C. Schappacher, Comput. Phys. Commun. **185**, 1529–1545 (2014). arXiv:1309.1692 [hep-ph]
124. S. Heinemeyer, C. Schappacher, Eur. Phys. J. C **77**(9), 649 (2017). arXiv:1704.07627 [hep-ph]
125. A. Djouadi, J.L. Kneur, G. Moultaka, Comput. Phys. Commun. **176**, 426 (2007). arXiv:hep-ph/0211331
126. Joint LEP2 SUSY Working Group, the ALEPH, DELPHI, L3 and OPAL Collaborations, see: http://lepsusy.web.cern.ch/lepsusy/
127. M. Mühlleitner, A. Djouadi, Y. Mambrini, Comput. Phys. Commun. **168**, 46 (2005). arXiv:hep-ph/0311167
128. J. Hisano, S. Matsumoto, M.M. Nojiri, O. Saito, Phys. Rev. D **71**, 015007 (2005). arXiv:hep-ph/0407168
129. C. Amole et al. (PICO), Phys. Rev. D **100**(2), 022001 (2019). arXiv:1902.04031 [astro-ph.CO]
130. E. Aprile et al. (XENON), Phys. Rev. Lett. **122**(14), 141301 (2019). arXiv:1902.03234 [astro-ph.CO]
131. E. Aprile et al. (XENON), JCAP **11**, 031 (2020). arXiv:2007.08796 [physics.ins-det]
132. D.S. Akerib et al. (LUX-ZEPLIN), Phys. Rev. D **101**(5), 052002 (2020). arXiv:1802.06039 [astro-ph.IM]
133. C.E. Aalseth et al. (DarkSide-20k), Eur. Phys. J. Plus **133**, 131 (2018). arXiv:1707.08145 [physics.ins-det]
134. M. Ibe, S. Matsumoto, R. Sato, Phys. Lett. B **721**, 252–260 (2013). arXiv:1212.5989 [hep-ph]
135. J. Billard et al. Rept. Prog. Phys. **85**(5), 056201 (2022). arXiv:2104.07634 [hep-ex]
136. F. Ruppin, J. Billard, E. Figueroa-Feliciano, L. Strigari, Phys. Rev. D **90**(8), 083510 (2014). arXiv:1408.3581 [hep-ph]
137. C. Bœhm, D.G. Cerdeño, P.A.N. Machado, A. Olivares-Del Campo, E. Perdomo, E. Reid, JCAP **01**, 043 (2019). arXiv:1809.06385 [hep-ph]
138. X. Cid Vidal et al., CERN Yellow Rep. Monogr. **7**, 585–865 (2019). arXiv:1812.07831 [hep-ph]
139. H. Baer et al., The international linear collider technical design report—volume 2: physics. arXiv:1306.6352 [hep-ph]
140. G. Moortgat-Pick et al., Eur. Phys. J. C **75**(8), 371 (2015). arXiv:1504.01726 [hep-ph]
141. L. Linssen, A. Miyamoto, M. Stanitzki, H. Weerts, arXiv:1202.5940 [physics.ins-det]
142. H. Abramowicz et al. (CLIC Detector and Physics Study Collaboration), arXiv:1307.5288 [hep-ex]
143. P. Burrows et al. (CLICdp and CLIC Collaborations), CERN Yellow Rep. Monogr. **1802**, 1 (2018). arXiv:1812.06018 [physics.acc-ph]
144. B. Fuks, M. Klasen, D.R. Lamprea, M. Rothering, Eur. Phys. J. C **73**, 2480 (2013). arXiv:1304.0790 [hep-ph]
145. G. Bozzi, B. Fuks, M. Klasen, Phys. Rev. D **74**, 015001 (2006). arXiv:hep-ph/0603074
146. G. Bozzi, B. Fuks, M. Klasen, Nucl. Phys. B **777**, 157–181 (2007). arXiv:hep-ph/0701202
147. J. Debove, B. Fuks, M. Klasen, Phys. Lett. B **688**, 208–211 (2010). arXiv:0907.1105 [hep-ph]
148. J. Debove, B. Fuks, M. Klasen, Nucl. Phys. B **842**, 51–85 (2011). arXiv:1005.2909 [hep-ph]
149. T. Barklow, J. Brau, K. Fujii, J. Gao, J. List, N. Walker, K. Yokoya, arXiv:1506.07830 [hep-ex]
150. K. Fujii et al., arXiv:1710.07621 [hep-ex]
151. S. Heinemeyer, C. Schappacher, Eur. Phys. J. C **78**(7), 536 (2018). arXiv:1803.10645 [hep-ph]
152. M. Berggren, arXiv:1308.1461 [hep-ph]
153. M.T.N. Pardo de Vera, M. Berggren, J. List, arXiv:2002.01239 [hep-ph]
154. M. Berggren, arXiv:2003.12391 [hep-ph]